A Parameter Identification Method for Dynamics of Lithium Iron Phosphate Batteries Based on Step-Change Current Curves and Constant Current Curves

Authors:

Zhichao He, Geng Yang, Languang Lu

Date Submitted: 2018-11-28

Keywords: constant current curves, step-change current curves, decouple, parameter identification

Abstract:

Parameterization of battery dynamics based on terminal operating data is a main concern in engineering applications of batteries. The key technology is designing an adequate test procedure and a data processing procedure to excite different inner dynamics and then estimate the parameters of a corresponding equivalent circuit model (ECM). This paper proposes a parameter identification method that utilizes the terminal voltage curves (TVC) under step-change current conditions and constant current conditions. With this method, I-V characteristics of battery's Ohmic resistance, mass diffusion process, thermal process and SOC varying process are decoupled and parametric functions of an ECM are obtained. Experimental results show that the method is easy to be implemented and modeling accuracy is sufficient for applications.

Record Type: Published Article

Submitted To: LAPSE (Living Archive for Process Systems Engineering)

Citation (overall record, always the latest version):	LAPSE:2018.1143
Citation (this specific file, latest version):	LAPSE:2018.1143-1
Citation (this specific file, this version):	LAPSE:2018.1143-1v1

DOI of Published Version: https://doi.org/10.3390/en9060444

energies

MDPI

Article

A Parameter Identification Method for Dynamics of Lithium Iron Phosphate Batteries Based on Step-Change Current Curves and Constant Current Curves

Zhichao He [1], Geng Yang [1,*] and Languang Lu [2]

[1] Department of Automation, Tsinghua University, Beijing 100084, China; hezc10@mails.tsinghua.edu.cn
[2] State Key Laboratory of Automotive Safety and Energy, Tsinghua University, Beijing 100084, China; lulg@tsinghua.edu.cn
* Correspondence: yanggeng@tsinghua.edu.cn; Tel.: +86-10-6279-2512

Academic Editor: Izumi Taniguchi
Received: 15 December 2015; Accepted: 30 May 2016; Published: 9 June 2016

Abstract: Parameterization of battery dynamics based on terminal operating data is a main concern in engineering applications of batteries. The key technology is designing an adequate test procedure and a data processing procedure to excite different inner dynamics and then estimate the parameters of a corresponding equivalent circuit model (ECM). This paper proposes a parameter identification method that utilizes the terminal voltage curves (TVC) under step-change current conditions and constant current conditions. With this method, *I-V* characteristics of battery's Ohmic resistance, mass diffusion process, thermal process and SOC varying process are decoupled and parametric functions of an ECM are obtained. Experimental results show that the method is easy to be implemented and modeling accuracy is sufficient for applications.

Keywords: parameter identification; decouple; step-change current curves; constant current curves

1. Introduction

Battery parameterization is important for engineering applications such as consistency evaluation, cell balancing and fault detection [1]. A lithium-ion battery can be considered as a multi-timescale dynamic system as shown in Figure 1. Under most operating conditions, inputs of the system are operating current and ambient temperature, and outputs of the system are terminal voltage and surface temperature. Dynamics inside the battery are Ohmic resistance, electrical double layer process, mass diffusion process, thermal process, SOC varying process, reversible process and ageing process [2]. These dynamics belong to different timescales and are often modeled with the equivalent circuit model (ECM) shown in Figure 2 [3]. In this ECM, electromotive force (EMF) is modeled as E, Ohmic resistance, electrical double layer process and mass diffusion process are modeled as R_0, $R_{ct}C_d$ branch and R_sC_s branch, and the remaining dynamics are considered as different factors that influences the ECM parameters. Therefore, battery parameterization is identification of the ECM parameters via external characteristics. For simplicity, lithium-ion battery dynamics within a charge/discharge cycle is considered in this paper, and the influences of reversible process and ageing process on battery's characteristics are neglected.

The relationship between different dynamics shown in Figure 3 can be built based on above discussion and existing researches [4–7]. In Figure 3, i is operating current, T_{amb} is ambient temperature, U is terminal voltage, T_{surf} is surface temperature, T_{in} is internal temperature, Z_{in} is internal impedance, E is EMF. Z_{in} is the key parameter determining battery's performance. This impedance reflects battery's Ohmic resistance, double layer process and mass diffusion process. As shown in the figure,

Z_{in} is a function of i, SOC and T_{in}. Therefore, the multiplication between i and Z_{in} determines the nonlinearity of a battery. SOC and T_{in} are outputs of SOC varying process and thermal process respectively. These two processes have similar timescales [3] and have major influence on Z_{in} [5,6]. Therefore, they are coupled and critical for ECM parameter identification.

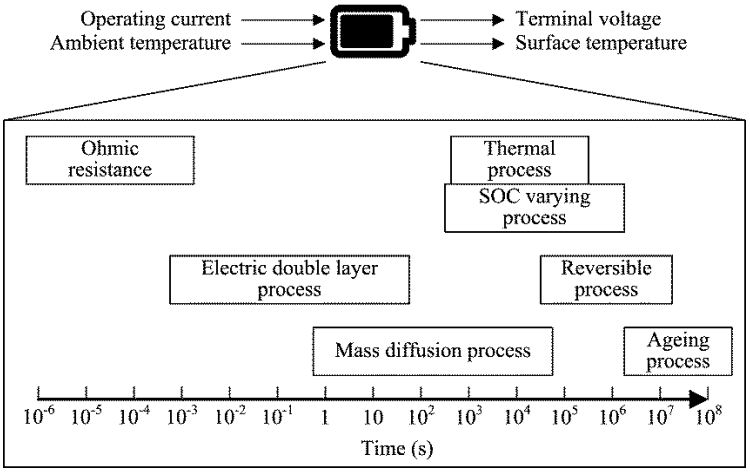

Figure 1. Systematic view of a battery.

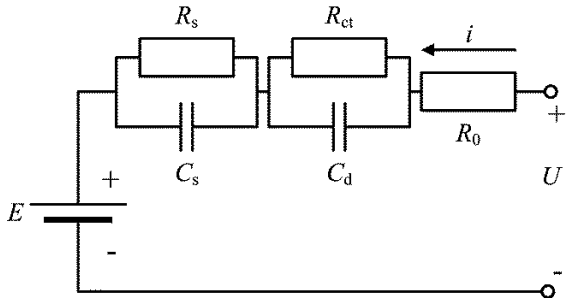

Figure 2. A typical equivalent circuit model for battery dynamics.

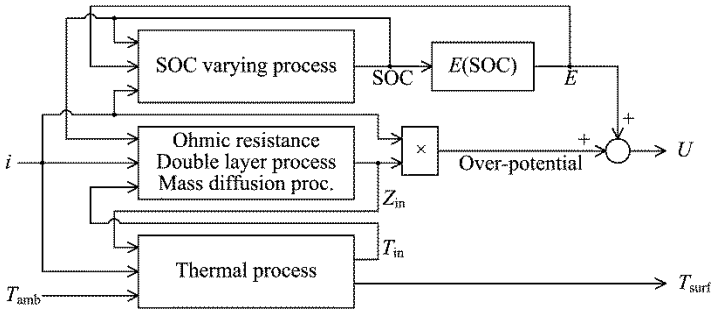

Figure 3. Relationship between different battery dynamics.

Modeling of SOC varying process is often accomplished through SOC estimation. Plenty of SOC estimation methods have been proposed under conditions of different current and ambient temperature, which have been critically reviewed by [7]. Essentially, these methods are all based on parameter identification of the ECM or current integration, and some of them have sufficient accuracy for applications. This paper utilizes ampere-hour counting method along with open circuit voltage estimation method for SOC estimation, which is similar with the method in [8–10]. Estimation error is verified with constant current discharge test to insure the accuracy.

Thermal process is the dynamic of a battery's internal temperature under different operating conditions. It is composed of heat generation process and heat transfer process, which are mainly determined by operating current and ambient temperature, respectively [11]. Several thermodynamic-based electrochemical models have been proposed for characterization of a battery [12–14] or battery pack [15–17]. These models highlight the general pattern of thermal process, but model parameters are obtained from typical experiments under laboratory conditions [18–21]. Battery's internal temperature has distinct influence on ECM parameters in Figure 2, therefore, variations of ECM parameters can be utilized to depict the thermal process, and then the TVC fitting method can be used for thermal characteristics modeling [22–27]. However, most papers focus on the relationship between ECM parameters and ambient temperature, and the thermal process excited by operating current is not sufficiently studied. Therefore, thermal behavior of a battery cannot be sufficiently characterized [28], which is needed for inconsistency evaluation [1] and heat propagation study for batteries [29]. Because the time scales of thermal process and SOC varying process are similar, it is necessary to design a method that decouples the processes and identifies the parameters. Conventional methods use extra current transients to obtain the variation of ECM parameters during a thermal process [25,26]. These methods take long time to characterize a thermal process, and introduce extra thermal processes, which makes parameter identification more complex. Therefore, a simpler method is needed for thermal process parameterization.

In engineering applications, parameter identification methods based on battery's *I*-*V* characteristics are preferred. One typical method is electrochemical impedance spectroscopy (EIS) test, which is suitable for material analysis and mechanism research [30–35]. Another method is terminal voltage curve (TVC) fitting, which utilizes system identification algorithms to calculate ECM parameters [36–38]. The TVC fitting method can be potentially implemented online under different operating conditions [39,40]. Therefore, it is more widely implemented in industry application [1].

It is clear from Figures 2 and 3 that estimating the parameters of the ECM is difficult because: (1) the ECM parameters are functions of many variations or factors such as operating current and SOC, and vice versa; (2) battery's TVCs are determined by the coupled dynamics in Figure 1, therefore, the ECM parameters need to be separated before being identified; (3) parameter identification requires sufficient transients as excitation, but suffers from redundant transients as disturbance. Therefore, a useful parameter identification method should include: (1) an adequate test procedure to obtain battery's TVCs which contain sufficient information of the dynamics; (2) a corresponding data processing procedure to extract the different dynamics inherent in TVCs and build the parametric functions while avoiding introducing redundant current transients to excite unwanted dynamics.

Based on above consideration, this paper proposes a parameterization method for battery's Ohmic resistance, mass diffusion process and thermal process under constant room temperature condition. Its purpose is to obtain battery parameters for performance evaluation, which is similar with the work in [41] or [42]. Therefore, offline experiments are implemented in this paper for battery test. Steps of the method are: (1) obtain a transient TVC with a step-change current test, which is the most simple dynamic current test with only one transient and sufficient constant current period for battery's thermal process; (2) extract and calculate ECM parameters with a data processing procedure utilizing constant current curves; (3) repeat Steps (1) and (2) with different current and transient points through battery's safe operating area (SOA) to obtain the parametric functions of the ECM. With this method, ECM parameters of any operating condition can be estimated via fitting and interpolation. The remainder of this paper is organized as follows. Section 2 introduces a modified ECM to depict battery's dynamics. Section 3 proposes parameter identification method for the ECM. Section 4 implements the method on a set of batteries and analyzes the results. Section 5 verifies the method under two multi-transients conditions. Section 6 summarizes the highlights of the method.

2. ECM Modification

As mentioned in Section 1, parameters of the ECM in Figure 2 are functions of SOC, current and internal temperature. If R_{ct} and C_d are neglected for simplicity, and the variation of R_0 and R_s caused by thermal process is decoupled as R_2, the second-order Thevenin ECM shown in Figure 4 can be built.

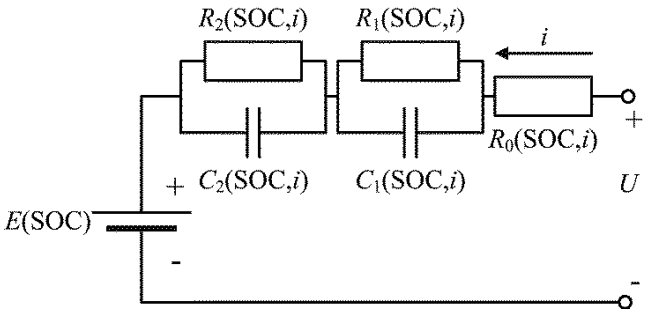

Figure 4. Modified the second-order Thevenin equivalent circuit model.

where R_0 is the Ohmic resistance; R_1 and C_1 are R_s and C_s, respectively; R_2 is the variance of direct current internal resistance (DCIR) caused by thermal process; R_2C_2 branch depicts battery's thermal process [26]. Because the temperature coefficient of battery's DCIR is negative [29], change direction of $R_0 + R_1$ caused by thermal process is always opposite with the change direction of battery's internal temperature or operating current transient. Therefore, value of R_2 is always negative.

Negative resistance is useful for depicting small-signal characteristics of nonlinear circuits [43,44]. Physically, a negative resistance depicts a circuit or device in which the change direction of the voltage across its terminal is opposite with the change direction of the current through it. While a positive resistance consumes power with positive current, a negative resistance produces power. For example, after a battery's operating current is increased, it causes an increasing component to the internal temperature and a decreasing component to DCIR, and then a decreasing component to power consumption. Decrease of power consumption caused by the increase of current can be considered as a virtual power source inside the battery, *i.e.*, the negative resistance R_2. In contrast, a decreasing current causes a decreasing component to the internal temperature and an increasing component to DCIR, and then an increasing component to power consumption. This also agrees with the characteristics of the virtual power source inside the battery. Therefore, small signal characteristics of battery's thermal process can be depicted with a negative resistance.

Negative capacitance is used to depict the nontrivial capacitance behaviors during small signal analysis of nonlinear circuits or devices, such as semiconductor devices [45]. It can be realized with negative impedance converter circuit [46]. Mathematically, negative capacitance can be considered as a capacitance with negative value and used for stability analysis [47]. However, there is still no sufficient analysis of its physical characteristics. In this paper, a negative capacitance, *i.e.*, C_2 is introduced to depict the positive time constant of thermal process with R_2C_2. Physical meaning of the capacitance remains to be analyzed.

3. Parameter Identification

This section proposes parameter identification method for the ECM in Figure 4. Step-change current tests are designed to obtain battery's transient *I-V* characteristics. Battery dynamics with large time constants can be excited and parameterized with the tests, because a step-change current curve has only one transient with abundant low frequency components, and redundant transients are not introduced. Procedure of the method is first elaborated under a set of $\{i_1, i_2, SOC_j\}$, which depicts the currents and transient point of a step-change current test. TVC of the battery is measured and ECM parameters of this condition are calculated. Then, above procedure is repeated under different sets of $\{i_1, i_2, SOC_j\}$ to

obtain parametric functions. These parametric functions can be used to estimate ECM parameters of any set of $\{i_1, i_2, \mathrm{SOC_j}\}$ via interpolation. Finally, some details are discussed.

3.1. Parameter Identification under a Set of $\{i_1, i_2, SOC_j\}$

Small-signal analysis is often used to calculate nonlinear resistances. Therefore, integration should be used to calculate the voltage over the resistance. For example, relationship between battery's Ohmic resistance and Ohmic polarization in Figure 4 is:

$$\begin{aligned} R_0\left(\mathrm{SOC}, i_1\right) &= \left.\frac{\mathrm{d}U_{R_0}(\mathrm{SOC},i)}{\mathrm{d}i}\right|_{i=i_1} \\ \Rightarrow U_{R_0}\left(\mathrm{SOC}, i_1\right) &= \int_0^{i_1} R_0\left(\mathrm{SOC}, i\right)\mathrm{d}i \end{aligned} \tag{1}$$

where U_{R0} is the voltage over R_0; and i_1 is the operating current. Equation (1) also indicates that obtaining parametric functions of the ECM is vital for battery modeling.

Suppose battery's SOC reaches $\mathrm{SOC_j}$ when time t is t_j under the constant current condition of i_1, then the step-change current test can be considered as a constant current test when t is less than t_j. It can be inferred from Figure 4 that battery's TVC under a constant current condition can be expressed as

$$U_{i_1}^{\mathrm{c}}\left(t\right) = E\left(\mathrm{SOC}\right) + \int_0^{i_1} \left[\begin{array}{ll} R_0\left(\mathrm{SOC}, i\right) & + \left(1 - e^{\frac{-t}{R_1(\mathrm{SOC},i)\cdot C_1(\mathrm{SOC},i)}}\right)\cdot R_1\left(\mathrm{SOC}, i\right) \\ & + \left(1 - e^{\frac{-t}{R_2(\mathrm{SOC},i)\cdot C_2(\mathrm{SOC},i)}}\right)\cdot R_2\left(\mathrm{SOC}, i\right) \end{array}\right] di \tag{2}$$

where i_1 is the operating current; terms in the square brackets depicts the Ohmic resistance, mass diffusion process and thermal process excited by the constant current curve.

Mass diffusion process can be considered at its steady state after a long-time constant current period. Then, Equation (2) can be simplified to Equation (3).

$$U_{i_1}^{\mathrm{c}}\left(t\right) = E\left(\mathrm{SOC}\right) + \int_0^{i_1}\left[R_0\left(\mathrm{SOC}, i\right) + R_1\left(\mathrm{SOC}, i\right) + \left(1 - e^{\frac{-t}{R_2(\mathrm{SOC},i)\cdot C_2(\mathrm{SOC},i)}}\right)\cdot R_2\left(\mathrm{SOC}, i\right)\right]\mathrm{d}i \tag{3}$$

At the time of t_j, i is switched from i_1 to i_2 via a step-change transient. Then battery's TVC can be expresses as:

$$\begin{aligned} U^{\mathrm{d}}\left(t\right)\big|_{t\geqslant t_\mathrm{j}} &= E\left(\mathrm{SOC}\right) + \int_0^{i_1}\left[R_0\left(\mathrm{SOC}, i\right) + R_1\left(\mathrm{SOC}, i\right) + \left(1 - e^{\frac{-t}{R_2(\mathrm{SOC},i)\cdot C_2(\mathrm{SOC},i)}}\right)\cdot R_2\left(\mathrm{SOC}, i\right)\right]\mathrm{d}i \\ &+ \int_{i_1}^{i_2}\left[R_0\left(\mathrm{SOC}, i\right) + \left(1 - e^{\frac{-(t-t_\mathrm{j})}{R_1(\mathrm{SOC},i)\cdot C_1(\mathrm{SOC},i)}}\right)R_1\left(\mathrm{SOC}, i\right) + \left(1 - e^{\frac{-(t-t_\mathrm{j})}{R_2(\mathrm{SOC},i)\cdot C_2(\mathrm{SOC},i)}}\right)\cdot R_2\left(\mathrm{SOC}, i\right)\right]\mathrm{d}i \end{aligned} \tag{4}$$

where the second line depicts the dynamics excited by the step-change transient. After a simple formulation, Equation (5) can be derived.

$$\begin{aligned} U^{\mathrm{d}}\left(t\right)\big|_{t\geqslant t_\mathrm{j}} &= E\left(\mathrm{SOC}\right) + \int_0^{i_2} R_0\left(\mathrm{SOC}, i\right)\mathrm{d}i \\ &+ \int_0^{i_2} R_1\left(\mathrm{SOC}, i\right)di - \int_{i_1}^{i_2} e^{\frac{-(t-t_\mathrm{j})}{R_1(\mathrm{SOC},i)\cdot C_1(\mathrm{SOC},i)}} R_1\left(\mathrm{SOC}, i\right)\mathrm{d}i \\ &+ \int_0^{i_1}\left(1 - e^{\frac{-t}{R_2(\mathrm{SOC},i)\cdot C_2(\mathrm{SOC},i)}}\right)\cdot R_2\left(\mathrm{SOC}, i\right)\mathrm{d}i + \int_{i_1}^{i_2}\left(1 - e^{\frac{-(t-t_\mathrm{j})}{R_2(\mathrm{SOC},i)\cdot C_2(\mathrm{SOC},i)}}\right)\cdot R_2\left(\mathrm{SOC}, i\right)\mathrm{d}i \end{aligned} \tag{5}$$

where the first line depicts battery's EMF and Ohmic polarization, second line depicts mass diffusion process and third line depicts thermal process.

Similarly, battery's constant current TVC under condition of i_2 can be derived from Equation (3):

$$U^{\mathrm{c}}_{i_2}(t) = E(\mathrm{SOC}) + \int_0^{i_2}\left[R_0(\mathrm{SOC},i) + R_1(\mathrm{SOC},i) + \left(1 - e^{\frac{-t}{R_2(\mathrm{SOC},i)\cdot C_2(\mathrm{SOC},i)}}\right)\cdot R_2(\mathrm{SOC},i)\right]\mathrm{d}i \quad (6)$$

Comparing Equation (5) with Equation (6), it can be indicated that: (1) EMF and Ohmic polarization remain same under both conditions; (2) mass diffusion process under the step-change current condition is superposed with a delayed exponentially-decaying transient excited by the current transient; and (3) thermal process under the step-change current condition is composed of two sub-processes excited by constant current period and the step-change current transient, respectively. Subtracting Equations (5) and (6) with SOC aligned, Equation (7) can be derived:

$$\begin{aligned} &U^{\mathrm{d}}(t) - U^{\mathrm{c}}_{i_2}(t)\Big|_{\mathrm{SOC}\geqslant\mathrm{SOC_j}} = -\int_{i_1}^{i_2} e^{\frac{-(t-t_{\mathrm{j}})}{R_1(\mathrm{SOC},i)\cdot C_1(\mathrm{SOC},i)}}\cdot R_1(\mathrm{SOC},i)\,\mathrm{d}i \\ &+\int_0^{i_2} e^{\frac{-(t-t_{\mathrm{j}}+t'_{\mathrm{j}})}{R_2(\mathrm{SOC},i)\cdot C_2(\mathrm{SOC},i)}}\cdot R_2(\mathrm{SOC},i)\,\mathrm{d}i - \int_0^{i_1} e^{\frac{-t}{R_2(\mathrm{SOC},i)\cdot C_2(\mathrm{SOC},i)}}\cdot R_2(\mathrm{SOC},i)\,\mathrm{d}i \\ &-\int_{i_1}^{i_2} e^{\frac{-(t-t_{\mathrm{j}})}{R_2(\mathrm{SOC},i)\cdot C_2(\mathrm{SOC},i)}}\cdot R_2(\mathrm{SOC},i)\,\mathrm{d}i \end{aligned} \quad (7)$$

where t'_{j} is the time when battery's SOC reaches $\mathrm{SOC_j}$ under the constant current condition of i_2. Relationship between t_{j} and t'_{j} will be shown with experimental results in Section 4.2.

Equation (7) is composed of two transient processes with amplitude and time constant varying with SOC, which shows the influence of battery's SOC varying process on the transient of mass diffusion process and thermal process, respectively. However, the influence also decreases exponentially with time, therefore it can be neglected and Equation (7) can be simplified to Equation (8):

$$\begin{aligned} &U^{\mathrm{d}}(t) - U^{\mathrm{c}}_{i_2}(t)\Big|_{\mathrm{SOC}\geqslant\mathrm{SOC_j}} = -\int_{i_1}^{i_2} e^{\frac{-(t-t_{\mathrm{j}})}{R_1(\mathrm{SOC_j},i)\cdot C_1(\mathrm{SOC_j},i)}}\cdot R_1(\mathrm{SOC_j},i)\,\mathrm{d}i \\ &+\int_0^{i_2} e^{\frac{-(t-t_{\mathrm{j}}+t'_{\mathrm{j}})}{R_2(\mathrm{SOC_j},i)\cdot C_2(\mathrm{SOC_j},i)}}\cdot R_2(\mathrm{SOC_j},i)\,\mathrm{d}i - \int_0^{i_1} e^{\frac{-t}{R_2(\mathrm{SOC_j},i)\cdot C_2(\mathrm{SOC_j},i)}}\cdot R_2(\mathrm{SOC_j},i)\,\mathrm{d}i \\ &-\int_{i_1}^{i_2} e^{\frac{-(t-t_{\mathrm{j}})}{R_2(\mathrm{SOC_j},i)\cdot C_2(\mathrm{SOC_j},i)}}\cdot R_2(\mathrm{SOC_j},i)\,\mathrm{d}i \end{aligned} \quad (8)$$

where all the parameters are constant.

Adding the over-potential caused by DCIR at $\mathrm{SOC_j}$ to Equation (8), Equation (9) can be derived:

$$\begin{aligned} &U^{\mathrm{d}}(t) - U^{\mathrm{c}}_{i_2}(t) + U^{\mathrm{c}}_{i_2}\left(t'_{\mathrm{j}}\right) - U^{\mathrm{c}}_{i_1}(t_{\mathrm{j}})\Big|_{\mathrm{SOC}\geqslant\mathrm{SOC_j}} \\ &= \int_{i_1}^{i_2}\left[\begin{array}{ll} R_0(\mathrm{SOC_j},i) & +\left(1 - e^{\frac{-(t-t_{\mathrm{j}})}{R_1(\mathrm{SOC_j},i)\cdot C_1(\mathrm{SOC_j},i)}}\right)\cdot R_1(\mathrm{SOC_j},i) \\ & +\left(1 - e^{\frac{-(t-t_{\mathrm{j}})}{R_2(\mathrm{SOC_j},i)\cdot C_2(\mathrm{SOC_j},i)}}\right)\cdot R_2(\mathrm{SOC_j},i) \end{array}\right]\mathrm{d}i \\ &+\int_0^{i_1} e^{\frac{-t_{\mathrm{j}}}{R_2(\mathrm{SOC_j},i)\cdot C_2(\mathrm{SOC_j},i)}}\cdot\left(1 - e^{\frac{-(t-t_{\mathrm{j}})}{R_2(\mathrm{SOC_j},i)\cdot C_2(\mathrm{SOC_j},i)}}\right)\cdot R_2(\mathrm{SOC_j},i)\,\mathrm{d}i \\ &-\int_0^{i_2} e^{\frac{-t'_{\mathrm{j}}}{R_2(\mathrm{SOC_j},i)\cdot C_2(\mathrm{SOC_j},i)}}\cdot\left(1 - e^{\frac{-(t-t_{\mathrm{j}})}{R_2(\mathrm{SOC_j},i)\cdot C_2(\mathrm{SOC_j},i)}}\right)\cdot R_2(\mathrm{SOC_j},i)\,\mathrm{d}i \end{aligned} \quad (9)$$

where the last two lines depict the difference of the thermal processes under different constant current conditions. This difference influences on impedance estimation and DCIR calculation. Under small-signal conditions, *i.e.*, i_1 is very close to i_2, Equation (10) can be derived.

$$\begin{aligned} & U^{\mathrm{d}}(t) - U_{i_2}^{\mathrm{c}}(t) + U_{i_2}^{\mathrm{c}}\left(t_{\mathrm{j}}'\right) - U_{i_1}^{\mathrm{c}}\left(t_{\mathrm{j}}\right)\Big|_{\mathrm{SOC}\geqslant\mathrm{SOC_j}} \\ \approx & \int_{i_1}^{i_2} \left[\begin{array}{c} R_0\left(\mathrm{SOC_j}, i\right) + \left(1 - e^{\frac{-(t-t_{\mathrm{j}})}{R_1(\mathrm{SOC_j},i)\cdot C_1(\mathrm{SOC_j},i)}}\right)\cdot R_1\left(\mathrm{SOC_j}, i\right) \\ + \left(1 - e^{\frac{-t_{\mathrm{j}}'}{R_2(\mathrm{SOC_j},i)\cdot C_2(\mathrm{SOC_j},i)}}\right)\cdot\left(1 - e^{\frac{-(t-t_{\mathrm{j}})}{R_2(\mathrm{SOC_j},i)\cdot C_2(\mathrm{SOC_j},i)}}\right)\cdot R_2\left(\mathrm{SOC_j}, i\right) \end{array} \right] \mathrm{d}i \end{aligned} \tag{10}$$

where a proportional coefficient constant with time exists in the last line. Compared with Equation (6), it can be indicated that relationship between identified R_2 and its true value is:

$$\hat{R}_2\left(\mathrm{SOC_j}, i\right) = \left(1 - e^{\frac{-t_{\mathrm{j}}'}{R_2(\mathrm{SOC_j},i)\cdot C_2(\mathrm{SOC_j},i)}}\right)\cdot R_2\left(\mathrm{SOC_j}, i\right) \tag{11}$$

Parameters in Equation (10) are constant and can be estimated with least square method. Detailed derivation of Equation (9) is given in Appendix A, derivation of Equation (10) is given in Appendix B, and detailed least square method is given in Appendix C.

It has to be noted that two assumptions are used in above procedure: (1) the influence of SOC varying process on the transient of mass diffusion process and thermal process can be neglected; and (2) i_1 is very close to i_2. The first assumption may cause modeling error with the variation of SOC, and will be discussed in Sections 4.2 and 4.4. The second assumption demands high accuracy of test bench and introduces a proportional coefficient to R_2. Considering the accuracy of our test bench, 2.6 A is selected as the minimal amplitude of step-change current.

3.2. Parameter Identification under Different Sets of {i_1, i_2, SOC_j}

The structure of ECM remains the same within SOA [1]. Therefore, the method described in Section 3.1 can be extended to different sets of {i_1, i_2, $\mathrm{SOC_j}$}. The whole procedures can be illustrated with Figure 5.

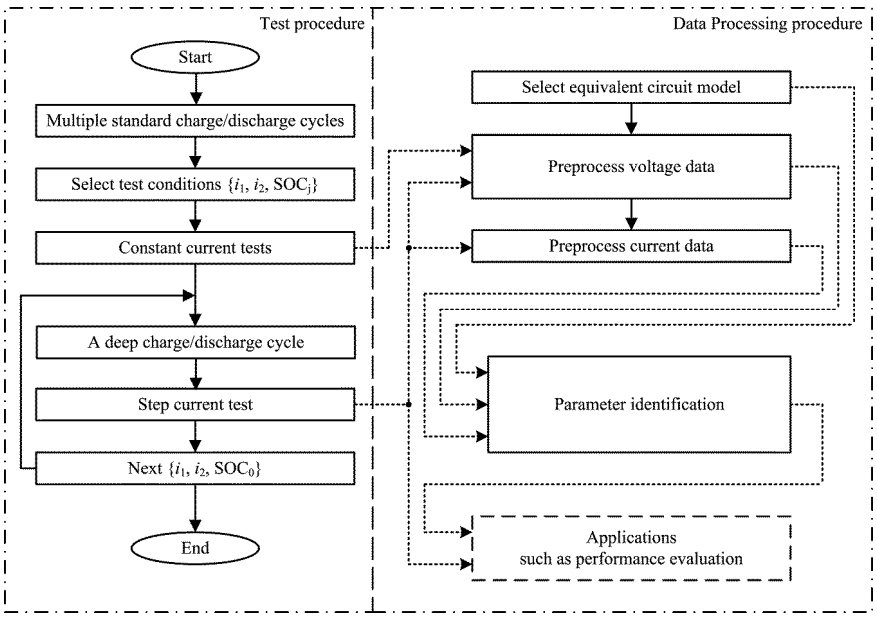

Figure 5. Parameter identification procedures.

ECM parameters under typical operating conditions can be obtained with the procedures. Relationships between parameters and current or SOC can be built with appropriate fitting method. Then, parametric functions can be obtained and ECM parameters of any set of $\{i_1, i_2, \mathrm{SOC_j}\}$ can be estimated via interpolation, which will be discussed in Sections 4.3 and 4.4.

3.3. Neglected Dynamics

Battery's reversible process and ageing process are neglected in Sections 3.1 and 3.2. These two dynamics reflect change of battery's characteristics with cycle number and influence the test results. Thus, the test procedure needs to be modified to improve modeling accuracy. Reversible process can be eliminated with some specific operations, such as the deep charge/discharge cycles placed before each step-change current test in Figure 5. Ageing process can be mitigated by reducing cycle number of each battery. Then, parameter identification method in Figure 5 needs be implemented on several batteries in parallel regardless of inconsistency between different batteries.

4. Experiments and Analysis

This section illustrates the procedures in Figure 5 on a set of lithium iron phosphate batteries. Basic parameters of batteries and test benches are first presented. Then, a set of parameters is identified and the errors are analyzed. In Sections 4.3 and 4.4, parameterization is conducted under different sets of $\{i_1, i_2, \mathrm{SOC_j}\}$ to build parametric functions. Finally, proposed method is verified under a set of $\{i_1, i_2, \mathrm{SOC_j}\}$ with all the ECM parameters estimated with proposed method.

4.1. Test Conditions

Eight brand new lithium iron phosphate batteries of a same batch are used for test to reduce the impact of the ageing process. Inconsistency of the batteries' capacity and DCIR are less than 0.5‰, which can be neglected. Detailed battery parameters, test environment and operating conditions are given in Table 1. As shown in the table, selected operating currents cover the entire SOA to provide a more complete view to batteries' nonlinearity; ambient temperature is fixed at the rated value to avoid its impact on the batteries' transient characteristics, especially on the thermal process. Only discharge conditions are implemented for simplicity. Parameter identification method for charge conditions is the same. 560 step-change current tests and 560 deep charge/discharge cycles are conducted in total, *i.e.*, less than 150 charge/discharge cycles for each battery. Capacity fading and DCIR variance caused by the test are less than 1% and 0.1‰, respectively, therefore impact of the ageing process can be neglected.

Table 1. Test conditions.

Item	Value
Battery parameters	-
Type and Batch No.	BAK 36800MP-Fe/2VF10L06 06877
Rated capacity (Ah)	6.5
Rated temperature (K)	298
Maximum charge current (A)	3.25
Maximum discharge current (A)	−19.5
Test environment	-
Test bench type	Neware CT-4008-5V100A-NTFA
Measurement range	0.01–5 V, 0.2–100 A
Measurement accuracy (%)	±0.0153
Sample rate (Hz)	1
Thermal chamber type	Jianhu JH-150F
Accuracy (K)	±1
Operating conditions	-
i_1 and i_2 (A)	1.3, 3.9, 6.5, 9.1, 11.7, 14.3, 16.9, 19.5
$\mathrm{SOC_j}$ (%)	10, 20, 30, 40, 50, 60, 70, 80, 90, 100
Ambient temperature (K)	298

4.2. Parameter Identification under a Set of {i_1, i_2, SOC_j}

Test results under a set of {i_1, i_2, SOC_j} are presented in this section. Modeling errors are analyzed and the method is validated. Results under {i_1 = −1.3 A, i_2 = −3.9 A, SOC_j = 79%} are chosen as an example and presented in Figure 6. Figure 6a shows the battery's operating current curve during step-change current test; Figure 6b shows the battery's TVCs under step-change current condition and −3.9 A constant current conditions, where the relationship between t_j and t_j' are also presented; Figure 6c,d shows the current curve and voltage residue curve obtained with the method in Section 3.1; Figure 6e shows battery's surface temperature under constant current and step-change current conditions; Figure 6f shows residue between the temperature curves in Figure 6e. It can be inferred from Figure 6d that the voltage residue curve of the lithium-ion battery shows a similar pattern to the coup-de-fouet curve of a lead-acid battery, which is composed of three components: a step-change caused by Ohmic resistance; a small timescale dynamic caused by mass diffusion process; a reversed large timescale dynamic caused by thermal process, which have the same time constant with the temperature curve in Figure 6f. ECM parameters R_0, R_1, C_1, R_2 and C_2 in Figure 4 can be calculated via least-square method with the curve in Figure 6c as input data and the curve in Figure 6d as output data.

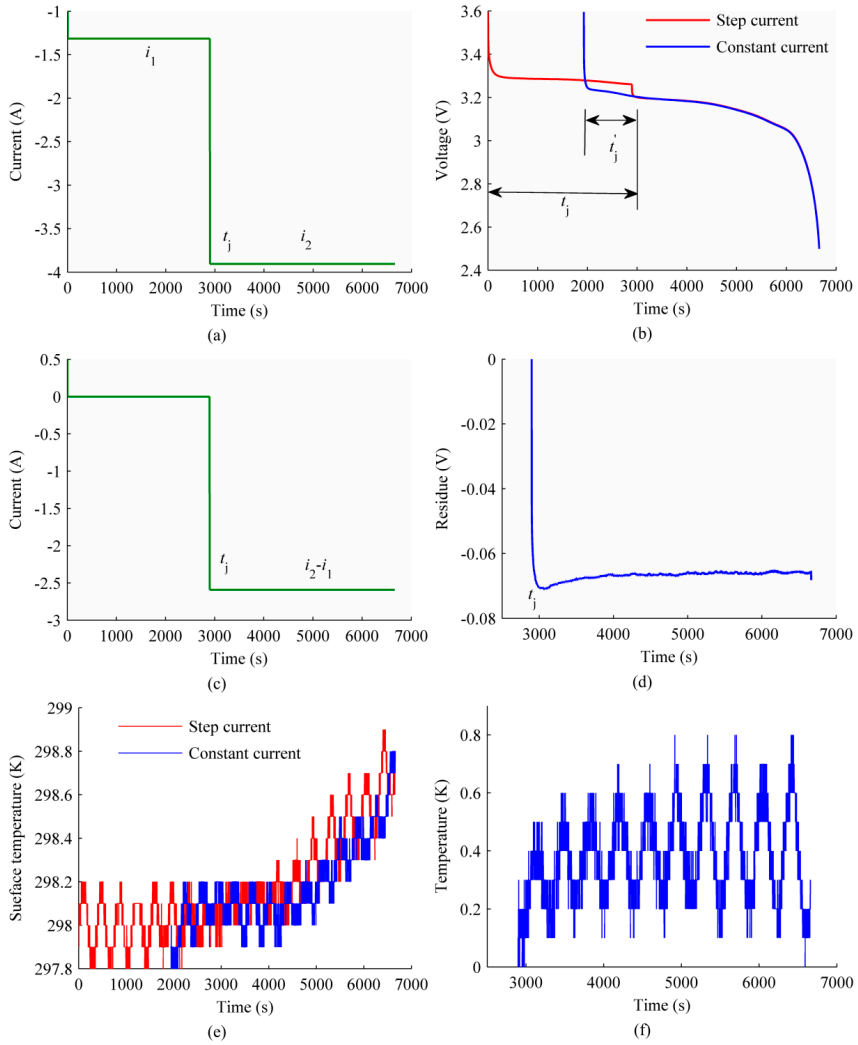

Figure 6. Test results under {i_1 = −1.3 A, i_2 = −3.9 A, SOC_j = 79%}: (**a**) Current curve; (**b**) Terminal voltage curves; (**c**) Preprocessed current curve; (**d**) Residue voltage curve; (**e**) Surface temperature curves; (**f**) Residue temperature curve.

It should be noted that compared with DCIR change, measured temperature change is smaller than the results given by existing researches such as [35] and [36]. It indicates that battery's surface temperature can hardly reflect the actual internal temperature, especially on cylindrical batteries, which have large radiating areas. Therefore, results in Figure 6e,f can only reflect the thermal process qualitatively despite the measurement noise. Quantitative analysis and modeling requires direct access to battery's internal temperature, which will be studied in the future.

Modeling results and its relative error are presented in Figure 7. The error remains less than 0.5‰when the battery's SOC is greater than 6%, which is almost the limit of laboratory test environment. Considering the fact that the battery's minimal SOC is 4.124% under the −3.9 A constant current condition, it can be concluded that proposed method has high accuracy during most of the battery's SOC range. Relatively larger errors exist near the step-change point and at low SOC. Detailed analysis of the errors is as follows.

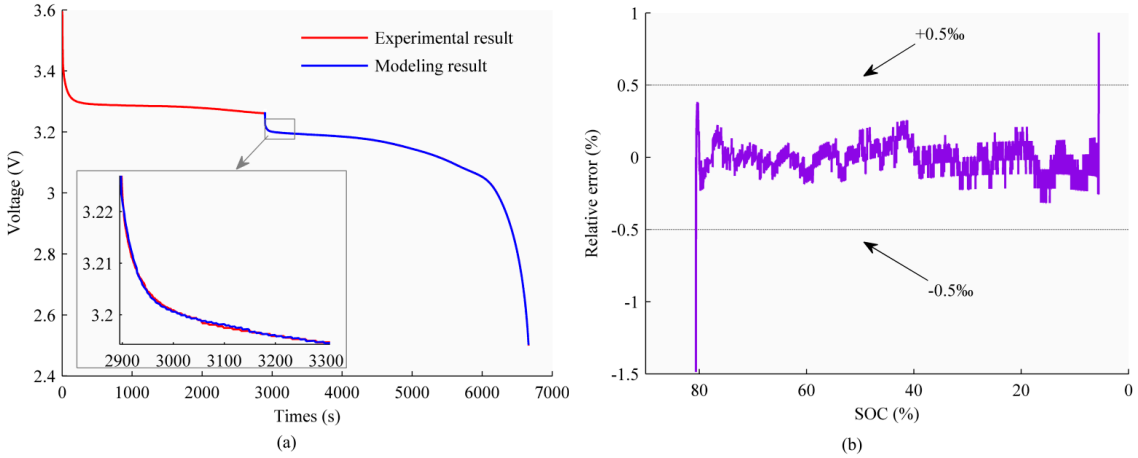

Figure 7. Modeling result under $\{i_1 = -1.3$ A, $i_2 = -3.9$ A, $SOC_j = 79\%\}$: (**a**) Terminal voltage curve estimation; (**b**) Relative error.

As mentioned in Section 2, battery's *I-V* characteristics near the transient point are mainly determined by Ohmic resistance and electrical double-layer process. The electrical double-layer process is neglected by the ECM in Section 3, which leads to the error near the transient point. A higher-order ECM, such as the third-order Thevenin model, can be used to reduce this error. However, because the error is less than 1.5‰, using a higher-order ECM leads to a minor improvement in accuracy but a major increase in complexity of parameter identification. Thus, a second-order Thevenin model is implemented in this paper.

The concentration of reactants inside a battery decreases continuously during a discharge process. When the battery is almost fully discharged, reactants at surface of electrodes are insufficient for redox reaction. As a consequence, battery's diffusion controlled current decreases as the Cottrell equation, and the mass diffusion polarization increases dramatically [48]. This process is not considered by the ECMs in this paper, which leads to the error at low SOC range.

Besides the above, there exists an error component that appears as a small oscillation near zero. This component is introduced by the assumption that the influence of SOC varying process on the transient of mass diffusion process and thermal process can be neglected. Because the least-square method is implemented for parameter identification, the error appears as a small oscillation near zero. Considering the error is no more than 0.5‰, which is acceptable in this paper, this assumption is valid. Modeling accuracy can be further improved by implementing appropriate identification methods for time-varying system, which will be studied in the future.

4.3. Parameter Identification under Different Sets of $\{i_1, i_2\}$

Relationships between ECM parameters and operating currents are presented and analyzed in this section. To facilitate elaboration, results under SOC_j = 80% are chosen as an example. Figure 8 presents the identification results, where x axis is absolute value of i_1, y axis is absolute value of i_2, z axis is value of corresponding parameter, dots are the original data, and surfaces are fitting results. 56 dots are presented in each figure for different sets of $\{i_1, i_2\}$ conditions. Some of the dots are behind the surface and hence invisible. Fitting surfaces are obtained with the 2-dimentional cubic spline interpolation method.

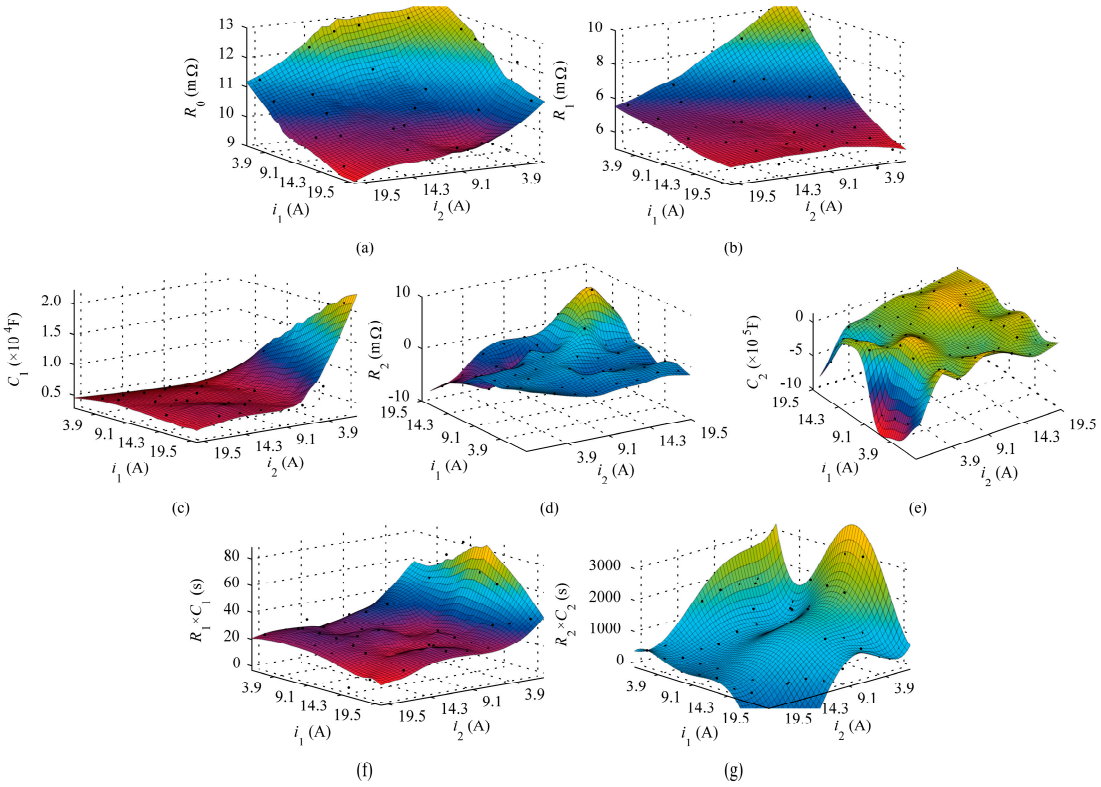

Figure 8. Identified (**a**) R_0; (**b**) R_1; (**c**) C_1; (**d**) R_2; (**e**) C_2; (**f**) $R_1 \times C_1$ and (**g**) $R_2 \times C_2$ under different sets of $\{i_1, i_2\}$ with the SOC_j as 80%.

Identification results of R_0 and R_1 are presented in Figure 8a,b, respectively, which show that the resistances decrease with operating current exponentially. The reason is: (1) identified R_0 and R_1 contain the neglected charge transfer resistance, which is determined by the Butler-Volmer equation; (2) R_0, R_1 and charge transfer resistance are influenced by battery's internal temperature, which is determined by the Arrhenius equation under constant ambient temperature conditions [29]. If the battery's internal temperature is obtained, parameters of the Arrhenius equation can be calculated, which is beneficial for evaluation of electrode materials.

Identification result of C_1 is presented in Figure 8c, which shows that value of C_1 is related to change direction of battery's operating current. Namely when i_1 is less than i_2, C_1 is approximately constant; when i_1 is greater than i_2, C_1 has positive correlation with $(i_1 - i_2)$. This also contributes to battery's nonlinearity including hysteresis.

Identification result of R_2 is presented in Figure 8d. When i_1 and i_2 are less than 0.6C, smaller results exists due to the instability of identification caused by the noise of measurement. When i_1 and i_2 are greater than 0.6C and less than 2.4C, a positive correlation can be found between the absolute value of R_2 and $(i_1 - i_2)$. It indicates that the change of battery's internal temperature in different

step-change current tests is different. Thus, R_2 can be used to estimate or predict the variance of internal temperature caused by operating current. When i_1 and i_2 are greater than 2.4C, false identification results arise. The reasons are: (1) battery's internal temperature is high when the operating current is large, which makes the variance of internal temperature excited by current transient relatively small or even unobservable; (2) discharge time under large current conditions is short, so evolution of thermal process is not sufficient before a battery reaches its cutoff condition. As a consequence, parameters of the thermal process become unidentifiable. To solve this problem, more detailed thermal models are needed and battery test procedure needs to be modified to sufficiently excite the thermal process.

Identification result of C_2 is presented in Figure 8e. C_2 has a positive correlation with i_2 while being approximately constant with i_1. It indicates that the transient characteristics of thermal process are mainly determined by the current after the transient point. Similarly, false values exist when i_1 and i_2 are greater than 2.4C, which has been discussed above.

Identified time constants of mass diffusion process and thermal process are presented in Figure 8f,g, respectively. Strong nonlinearity is shown in the figures. It has to be noted that change direction of current has distinct influence on the time constants, which is mainly introduced by C_1 and C_2 according to Figure 8c,e. This influence manifests as battery's nonlinearity, especially hysteresis. Thus, structure of the ECM can be improved and more detailed mechanism needs to be considered for a better accuracy, which will be studied in the future. Besides, negative time constants exist in Figure 8g under large current conditions. As discussed above, this is caused by the un-identifiability of ECM parameters. To solve this problem, parameter identification method needs to be improved to extend its validity.

4.4. Parameter Identification under Different SOC_j

Relationships between ECM parameters and SOC are presented and analyzed in this section. As discussed in Section 4.3, C_1 and C_2 are sensitive to the change direction of current transient. Therefore, identification results under two sets of $\{i_1, i_2\}$ are presented and analyzed.

Identification results under $\{i_1 = -14.3$ A, $i_2 = -1.3$ A$\}$ are presented in Figure 9. Dots are original values, and curves are fitting results. A smaller i_2 is chosen to ensure that there is sufficient time for battery's thermal process between the current transient and cut-off point, and then R_2 and C_2 can be identified. Identified parameters are fitted with following equation for a better accuracy:

$$\psi = a \cdot \exp(b \cdot \mathrm{SOC}) + c \cdot \exp(d \cdot \mathrm{SOC}) \tag{12}$$

where, ψ is ECM parameters such as R_0 or C_1; a, b, c and d are fitting coefficients.

Identification results of R_0, R_1 and R_2 are presented in Figure 9a,b,d, respectively. The absolute values of these resistances increase during discharge, among which R_0 and R_1 (*i.e.*, DCIR) have been discussed by Hu [49]. According to battery's thermal model [29], increase of DCIR leads to increase of: (1) variance of DCIR caused by the same variance of the internal temperature; (2) variance of the internal temperature caused by the same variance of operating current. As a consequence, absolute value of the battery's R_2 increases during discharge.

Identification results of C_1 and C_2 are presented in Figure 9c,e, respectively. The absolute values of C_1 and C_2 decrease during discharge. This decrease leads to the variation of time constants of mass diffusion process and thermal process as shown in Figure 9f,g, respectively, and leads to the oscillation error discussed in Section 4.2.

Identification results under $\{i_1 = -3.9$ A, $i_2 = -19.5$ A$\}$ are presented in Figure 10 as a comparison with the results in Figure 9.

From Figure 10, three major differences can be seen: (1) absolute values of C_1 and C_2 increase during discharge; (2) time constants of mass diffusion process and thermal process increase during discharge; (3) false values of R_2 and C_2 exist when $\mathrm{SOC_j}$ is less than 40%, which leads to the false values of the identified time constant of thermal process. The reason of first two differences is the nonlinear nature of mass diffusion process and thermal process, *i.e.*, the values of C_1 and C_2 are influenced by the change direction of operating current. The reason of the third difference is the insufficiency of

excitation on battery's thermal process, which specifically means that the interval between current transient and cut-off point is not sufficient for battery's thermal process. To improve the method, test procedure needs to be modified for a persistent excitation of battery dynamics within SOA.

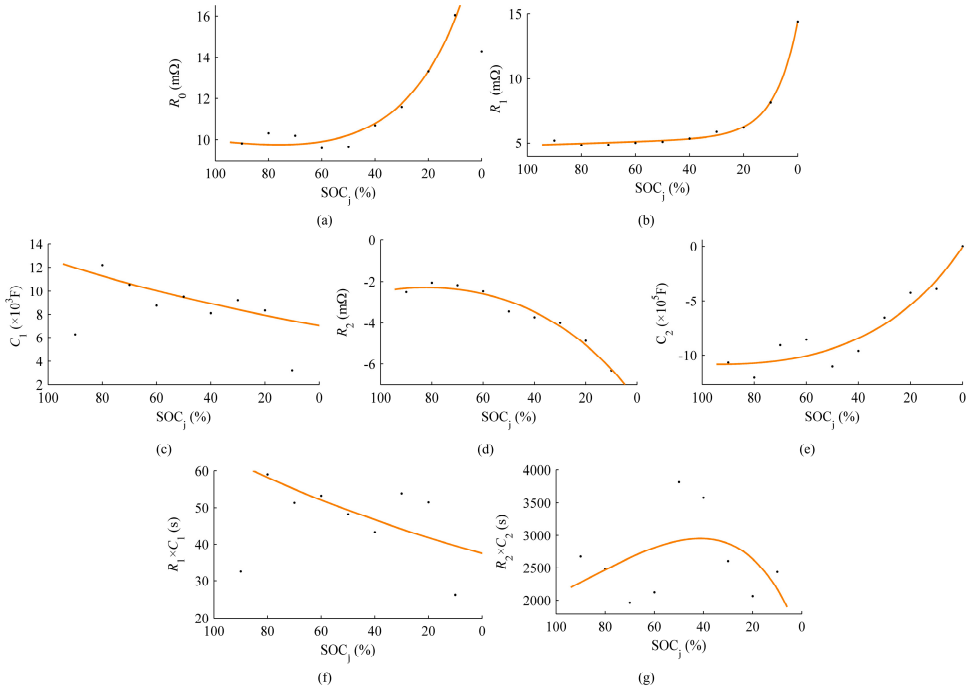

Figure 9. Identified (**a**) R_0; (**b**) R_1; (**c**) C_1; (**d**) R_2; (**e**) C_2 (**f**) $R_1 \times C_1$ and (**g**) $R_2 \times C_2$ under $\{i_1 = -14.3$ A, $i_2 = -1.3$ A$\}$.

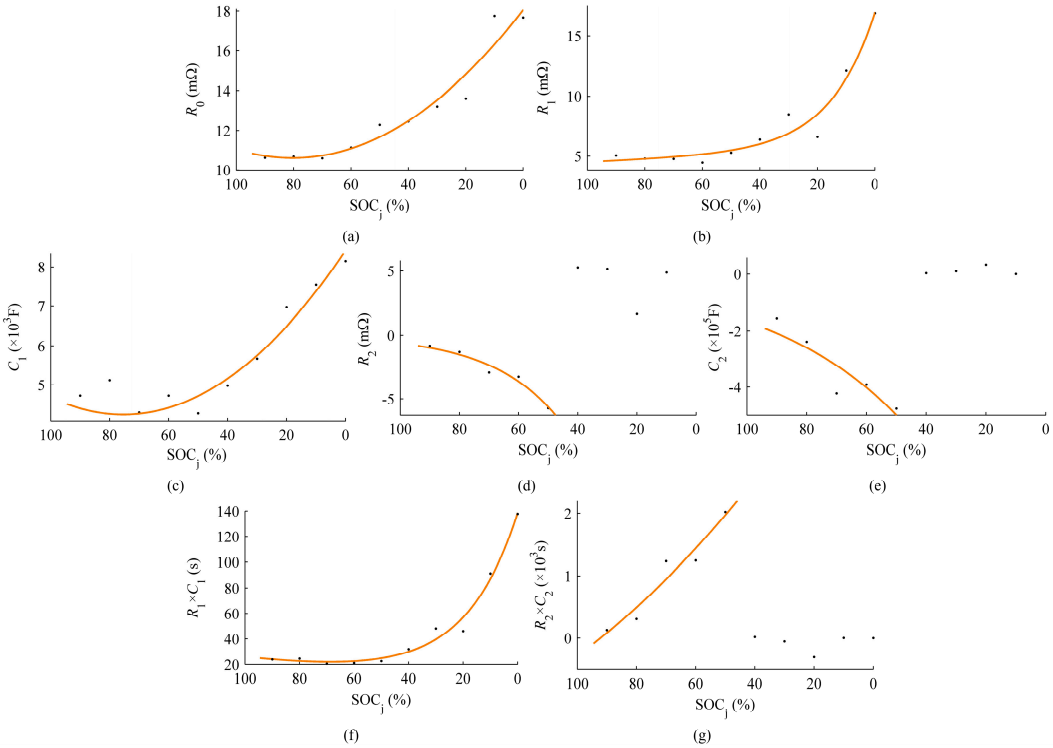

Figure 10. Identified (**a**) R_0; (**b**) R_1; (**c**) C_1; (**d**) R_2; (**e**) C_2; (**f**) $R_1 \times C_1$ and (**g**) $R_2 \times C_2$ under $\{i_1 = -3.9$ A, $i_2 = -19.5$ A$\}$.

4.5. Verification under {$i_1 = -13$ A, $i_2 = -10$ A, $SOC_j = 71\%$}

Verification results under {i_1 = −13 A, i_2 = −10 A, SOC_j = 71%} are presented in Figure 11. ECM parameters used for this verification are estimated with the identification results obtained in Section 3.2 and the interpolation methods mentioned in Sections 4.3 and 4.4. Optimal ECM parameters are calculated with the method in Section 3.1 for comparison, as listed in Table 2.

Table 2. Verification result.

Item	Optimal Value	Estimated Value	Relative Error (%)
R_0 (mΩ)	10.803	10.733	−0.648
R_1 (mΩ)	4.236	4.257	0.496
C_1 ($\times 10^3$ F)	6.156	6.707	8.591
$R_1 \times C_1$ (s)	26.077	28.552	9.491
R_2 (mΩ)	−2.349	−2.692	14.602
C_2 ($\times 10^5$ F)	−2.634	−1.914	−27.335
$R_2 \times C_2$ (s)	618.734	515.214	−16.731

As shown in Figure 11a,b, modeling error remains about −0.05% at the most SOC range. The error shows a unitary bias, which is different from the result in Figure 7. As can be indicated from Table 2, larger estimation errors exist on C_1, R_2 and R_2. As a consequence, time constants of mass diffusion process and thermal process are not accurately estimated, which can be intuitively observed in Figure 11c. Specifically, over-estimation of $R_1 \times C_1$ causes the peak of error curve at SOC of about 76%, which partially compensates the estimation error of R_2 and C_2; over-estimation of R_2 causes the bias at the most SOC range; over-estimation of $R_2 \times C_2$ causes the evolution of the error curve at SOC range between 65% and 50%.

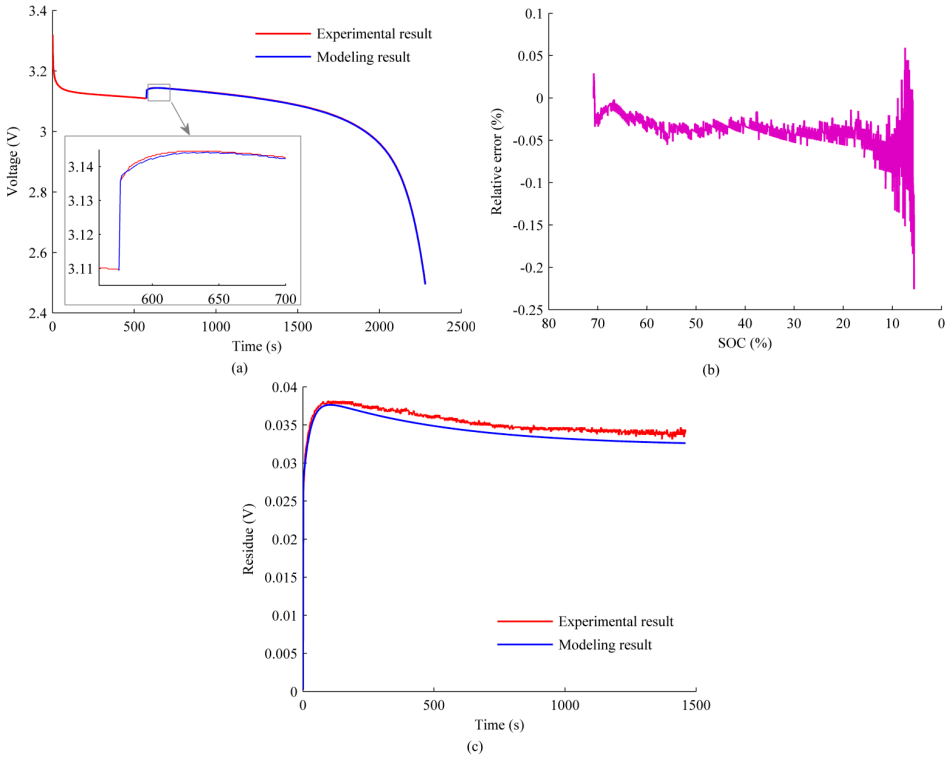

Figure 11. Modeling result under {i_1 = −13 A, i_2 = −10 A, SOC_j = 71%}: (**a**) Terminal voltage curve estimation; (**b**) Relative error; (**c**) Residue curve.

It has to be noted that although the estimation error of R_2 and C_2 are larger than 10% and 25%, respectively, error of TVC estimation is no more than 0.7% at most SOC ranges. The reason is that R_2

is relatively small compared with R_0 and R_1. Therefore, impact of R_2 and C_2 identification error on battery modeling is minor. On the other hand, it indicates that thermal parameter estimation requires high accuracy of TVC measurement and enough amplitude of current transient excitation.

5. Verification under DST (Dynamic Stress Test) and FUDS (Federal Urban Driving Schedule)

Verification of the method under DST (Dynamic Stress Test) and FUDS (Federal Urban Driving Schedule) [41] is presented in this section. Original DST and FUDS profiles are modified with power demand substituted by operating current. This aims to provide a complete access to battery's characteristics within SOA. Impact of this modification on experimental results can be neglected, because the constant current TVCs of lithium iron phosphate batteries are very flat.

An extended Kalman filter (EKF) based method [39] is reproduced for comparison. This method adopts the second-order Thevenin ECM to depict battery's Ohmic resistance, electrical double-layer process and mass diffusion process. ECM parameters are obtained with an adaptive EKF. The method proposed in this paper uses the second-order Thevenin ECM to depict battery's Ohmic resistance, mass diffusion process and thermal process, and calculates ECM parameters with least-square method with SOC varying process decoupled. In summary, these two methods consider battery dynamics of different timescales.

5.1. Data Processing Procedure under Multi-Transients Conditions

Key to the data processing procedure is decoupling battery's I-V characteristics of different dynamics. Constant current TVCs are utilized in Section 3.1, because they have the same SOC varying process with step-change current test curves. Operating conditions with multiple transients can be considered as conditions consist of a series of step-change transients. Under these conditions, piecewise constant current TVCs with proper SOC varying processes can be used to decouple thermal process. These TVCs can be generated with battery's constant current TVCs and estimated SOC curve under the multi-transients condition.

It must be noted that multiple battery dynamics of different SOC are coupled under multi-transients conditions. It introduces SOC varying process and nonlinearity to data processing results, which makes the ECM in Figure 4 time-varying and less accurate. A sliding window least square method with window width of 1000 s is adopted in this section. Besides, the proportional coefficient in Equation (10) is difficult to be accurately calculated under multi-transients conditions. Therefore, direct identification results are presented in this section. This simplification has no influence on identified time constants of battery dynamics.

5.2. Verification under DST

DST is a typical benchmark for battery testing [41]. A DST cycle lasts for 360 s, containing 20 transients. In this section, DST is implemented on a fully charged battery with 3.25 A as the maximum charge current and −19.5 A as the maximum discharge current. These currents cover the battery's entire SOA. 22 DST cycles are accomplished until the battery is fully discharged. The battery's surface temperature and terminal voltage remain within SOA during experiment.

Test results are presented in Figure 12, including the operating current curve of a cycle in Figure 12a and TVCs in Figure 12b. Piecewise constant current curve generated with constant current curves are also presented Figure 12b. Residue curve between the TVCs is used to estimate ECM parameters. Modeling results and relative errors are presented in Figure 12c,d, respectively.

As shown in Figure 12, when t is less than 6000, maximum and average errors of the EKF are 2.32% and 0.14%, respectively, and the errors of the proposed method are 2.24% and 0.12%, respectively. Both methods show good accuracy on predicting battery's I-V characteristics. When t is larger than 6000, larger errors exist on both methods and EKF does not converge on some transients. This is caused by battery's strong nonlinearity and fast time-varying characteristics at low SOC range, which makes the algorithms less accurate.

It must be noted that a different trend exists on the voltage curve estimated by the proposed method at time of about 3300 s. It is modeling error caused by parameter identification inaccuracy. Specifically, battery's SOC and equivalent current used for parameter identification varies when the sliding window moves, and then identified parameters varies. This variation changes the output of ECM and causes modeling error. Because proposed method concerns battery dynamics with larger time constants, so dynamics of small time constant are neglected and correction of modeling errors takes longer time than EKF, which considers the double layer process. To solve this problem, proposed method needs to be improved with battery dynamics of smaller time constants considered.

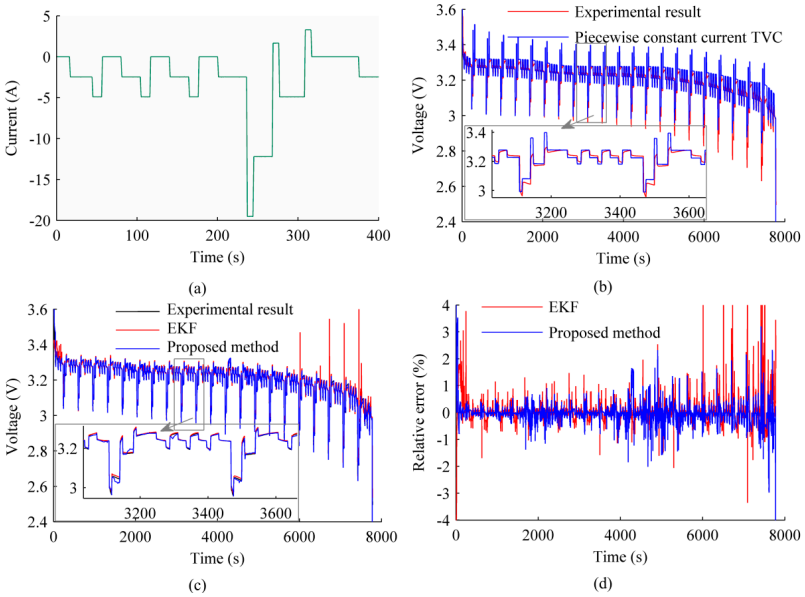

Figure 12. (**a**) Current curve (a cycle); (**b**) TVCs; (**c**) Modeling results and (**d**) Modeling error under DST.

Parameter identification results are presented in Figure 13. Initial values of the parameters are set to zero before parameter identification. Because of lack of data, beginning 1000 s of the results is set to the values identified with beginning 1000 s of experimental data via one-time least square method to present the general value of each parameter.

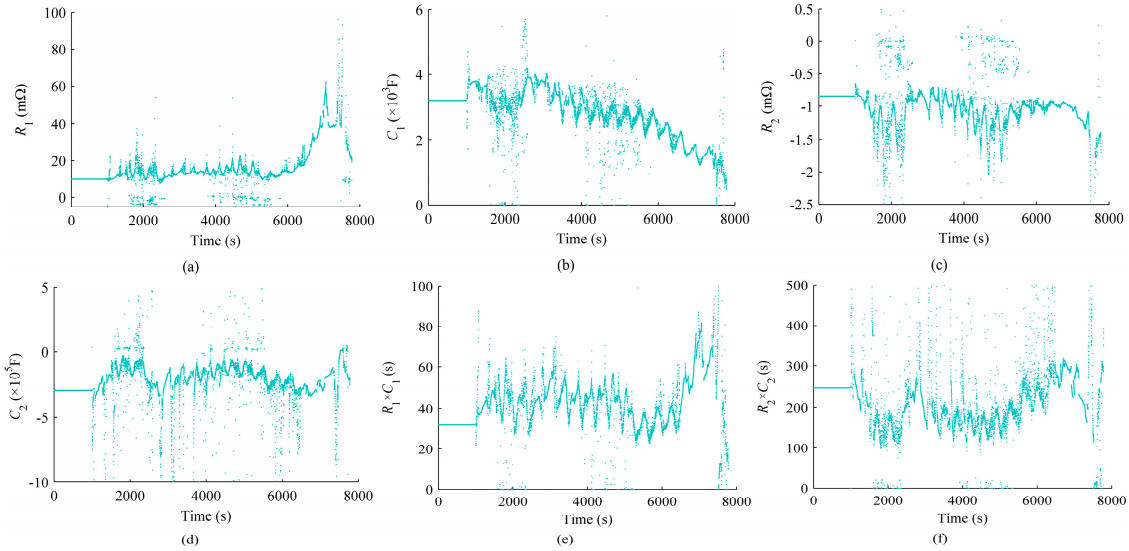

Figure 13. Identified (**a**) R_1; (**b**) C_1; (**c**) R_2; (**d**) C_2; (**e**) $R_1 \times C_1$ and (**f**) $R_2 \times C_2$ under DST.

A periodical oscillation superposed with a dynamic with larger time scale is shown in the figure. The oscillation is caused by the periodical variation of operating current. The large time scale dynamic is caused by SOC varying process and thermal process. Identification results remain stable until the battery is almost fully discharged. It indicates that DST profile is capable to excite battery's thermal process sufficiently at low SOC range, which ensures the identifiability of R_2 and C_2. Few false values exist when the operating current is large. It indicates that the identifiability problem under large current conditions remains to be solved.

5.3. Verification under FUDS

FUDS is a test benchmark close to actual vehicle operating conditions [41]. A FUDS cycle lasts for 1373 s, containing numerous transients. In this section, FUDS is implemented on a fully charged battery with 3.25 A as the maximum charge current and −19.5 A as the maximum discharge current. Five FUDS cycles are accomplished before the battery is fully discharged. The battery's surface temperature and terminal voltage remain within SOA during experiment.

Test results are presented in Figure 14, where the operating current curve of a FUDS cycle and TVCs are presented in Figure 14a,b, respectively. It must be noted that an average error of 3.32% arises between the piecewise constant current curve and the experimental result after 5700 s. It indicates that the influence of SOC varying process and thermal process on DCIR under FUDS is different from that under constant current conditions. However, this error causes a minor impact on the modeling results, which will be discussed later. Modeling results and relative error are presented in Figure 14c,d, respectively. When t is less than 6500 and despite the points of divergence, maximum and average errors of EKF are 1.95% and 0.09%, respectively, and the errors of proposed method are 1.51% and 0.07%, respectively. Compared with the results under DST, the errors of the conventional method are increased by 12.9% and 35.7%, and the errors of the proposed method are decreased by 31.8% and 30.0%. It indicates that FUDS is more informative for parameter identification of the ECM. Similar with the results under DST, large errors or even divergence exist at some drastic transient points of the methods. Therefore, a set of better coefficients or even a better algorithm is needed to improve the modeling accuracy.

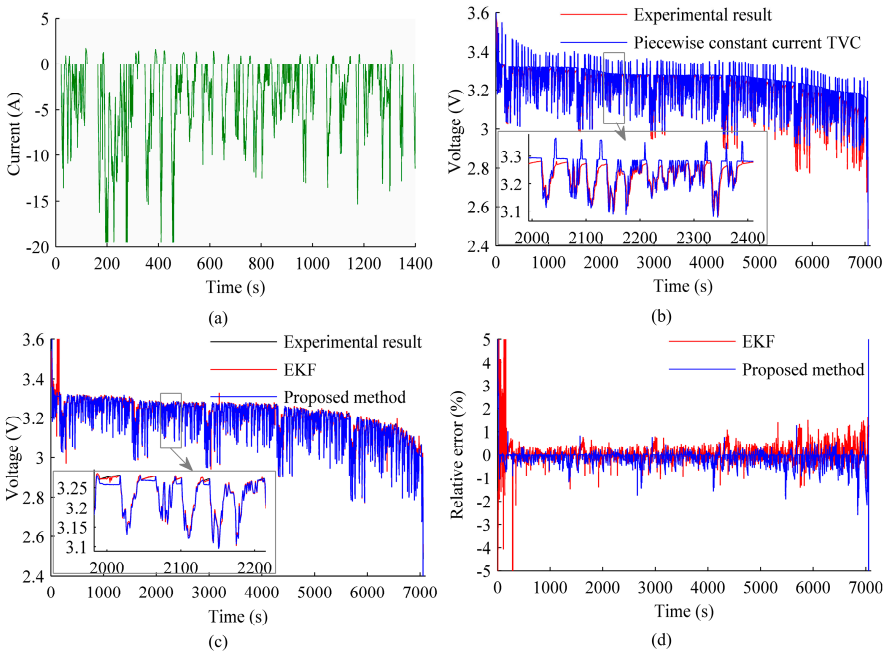

Figure 14. (**a**) Current curve (a FUDS cycle); (**b**) TVCs; (**c**) Modeling results and (**d**) Modeling error FUDS.

Parameter identification results are presented in Figure 15. Same with Figure 13, beginning 1000 s of the results is set to the values identified with beginning 1000 s of experimental data via one-time least square method to present the general value of each parameter. Initial values of the parameters are set to zero before parameter identification, *i.e.*, the convergence procedures of parameter identification are not shown in the figure. Similar with the results under DST, identified parameters vary periodically with operating current. As shown in the figure, R_2 and C_2 can be identified in a wider SOC range than in Figure 13. It indicates that FUDS is more informative for battery parameter identification.

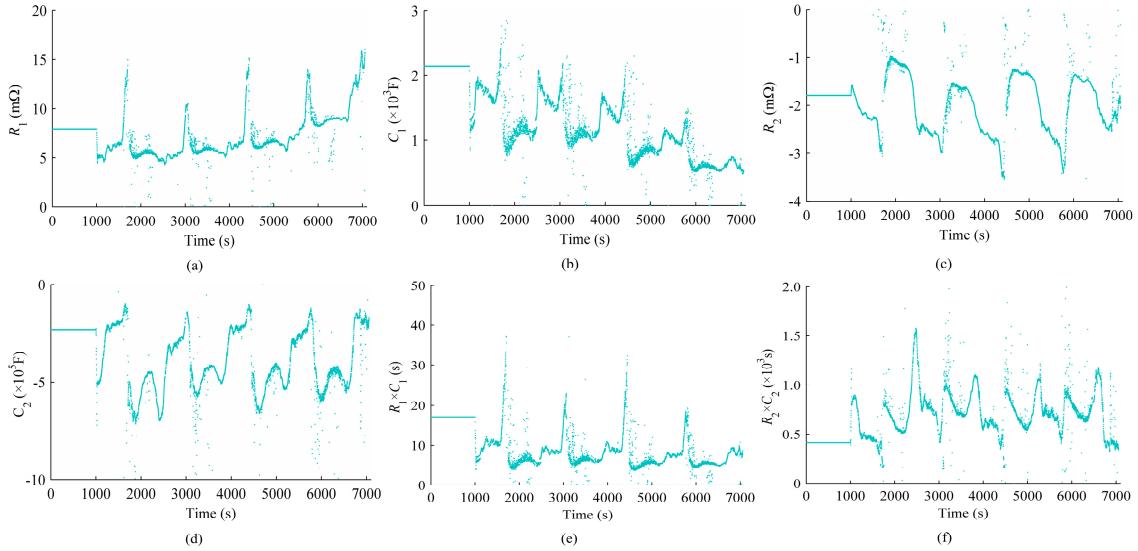

Figure 15. Identified (**a**) R_1; (**b**) C_1; (**c**) R_2; (**d**) C_2; (**e**) $R_1 \times C_1$ and (**f**) $R_2 \times C_2$ under FUDS.

It must be noted that identified time constant under FUDS are slightly different than the results under DST. Specifically, identified $R_1 \times C_1$ becomes smaller and identified $R_2 \times C_2$ becomes larger. The reasons may be: (1) Equivalent operating current of DST and FUDS are different, then ECM parameters are different; (2) Amplitudes of current transients of DST and FUDS are different, then the errors introduced during data processing are different; (3) Battery's internal temperature under DST and FUDS are different, then ECM parameters are different. Detailed analysis requires sufficient information of battery's internal temperature and thorough analysis of parameter identification algorithms, which are beyond the scope of this paper.

6. Conclusions

This paper proposes a parameter identification method for battery dynamics depicted by the ECM in Figure 4. Highlights of the method are as follows compared with conventional methods.

(1) An adequate test procedure is designed which includes step-change current tests and constant current tests. Therefore, battery dynamics can be sufficiently excited without introducing redundant excitations.

(2) A corresponding data processing procedure is designed to extract battery dynamics including thermal process inherent in *I*-*V* characteristics, and then estimate the parameters of ECM, which are functions of current and SOC. Experimental results show that accuracy of the parameterization is sufficient.

ECM parametric functions covering battery's SOA can be obtained with this method through a set of offline experiments. These parametric functions are beneficial for many engineering applications such as performance evaluation and consistency evaluation of different batteries. This paper focuses on the formulation and verification of parameter identification method, so offline experiments are

implemented. Improvements of the method, such as weakening the assumptions, extending the validity and improving the algorithm, will be studied in the future.

Acknowledgments: This research is funded by the National High Technology Research and Development Program of China under Grant 2012AA050217 and 2015AA050606, and the National Natural Science Foundation of China (NSFC) under Grant 61273045 and 51361135705.

Author Contributions: Zhichao He proposed the original idea; he also conceived, designed and carried out the experiments, and analyzed the data; Geng Yang and Zhichao He developed the essential idea behind the research, and prepared the manuscript. Languang Lu verified the theories, and corrected the manuscript.

Conflicts of Interest: The authors declare no conflict of interest.

Appendix A. Derivation of Equation (9)

$$
\begin{aligned}
&U^{\mathrm{d}}(t) - U^{\mathrm{c}}_{i_2}(t) + U^{\mathrm{c}}_{i_2}\left(t'_{\mathrm{j}}\right) - U^{\mathrm{c}}_{i_1}\left(t_{\mathrm{j}}\right)\Big|_{\mathrm{SOC}\geqslant\mathrm{SOC_j}} \\
&= -\int_{i_1}^{i_2} e^{\frac{-(t-t_{\mathrm{j}})}{R_1(\mathrm{SOC_j},i)\cdot C_1(\mathrm{SOC_j},i)}} \cdot R_1\left(\mathrm{SOC_j},i\right)\mathrm{d}i \\
&+\int_0^{i_2} e^{\frac{-(t-t_{\mathrm{j}}+t'_{\mathrm{j}})}{R_2(\mathrm{SOC_j},i)\cdot C_2(\mathrm{SOC_j},i)}} \cdot R_2\left(\mathrm{SOC_j},i\right)\mathrm{d}i - \int_0^{i_1} e^{\frac{-t}{R_2(\mathrm{SOC_j},i)\cdot C_2(\mathrm{SOC_j},i)}} \cdot R_2\left(\mathrm{SOC_j},i\right)\mathrm{d}i \\
&-\int_{i_1}^{i_2} e^{\frac{-(t-t_{\mathrm{j}})}{R_2(\mathrm{SOC_j},i)\cdot C_2(\mathrm{SOC_j},i)}} \cdot R_2\left(\mathrm{SOC_j},i\right)\mathrm{d}i \\
&+E\left(\mathrm{SOC_j}\right) + \int_0^{i_2}\left[R_0\left(\mathrm{SOC_j},i\right) + R_1\left(\mathrm{SOC_j},i\right) + \left(1 - e^{\frac{-t'_{\mathrm{j}}}{R_2(\mathrm{SOC_j},i)\cdot C_2(\mathrm{SOC_j},i)}}\right)\cdot R_2\left(\mathrm{SOC_j},i\right)\right] \\
&-E\left(\mathrm{SOC_j}\right) - \int_0^{i_1}\left[R_0\left(\mathrm{SOC_j},i\right) + R_1\left(\mathrm{SOC_j},i\right) + \left(1 - e^{\frac{-t_{\mathrm{j}}}{R_2(\mathrm{SOC_j},i)\cdot C_2(\mathrm{SOC_j},i)}}\right)\cdot R_2\left(\mathrm{SOC_j},i\right)\right] \\
&= \int_{i_1}^{i_2}\left[\begin{array}{r} R_0\left(\mathrm{SOC_j},i\right) + \left(1 - e^{\frac{-(t-t_{\mathrm{j}})}{R_1(\mathrm{SOC_j},i)\cdot C_1(\mathrm{SOC_j},i)}}\right)\cdot R_1\left(\mathrm{SOC_j},i\right) \\ + \left(1 - e^{\frac{-(t-t_{\mathrm{j}})}{R_2(\mathrm{SOC_j},i)\cdot C_2(\mathrm{SOC_j},i)}}\right)\cdot R_2\left(\mathrm{SOC_j},i\right)\end{array}\right]\mathrm{d}i \\
&+\int_0^{i_2} e^{\frac{-(t-t_{\mathrm{j}}+t'_{\mathrm{j}})}{R_2(\mathrm{SOC_j},i)\cdot C_2(\mathrm{SOC_j},i)}} \cdot R_2\left(\mathrm{SOC_j},i\right)\mathrm{d}i - \int_0^{i_1} e^{\frac{-t}{R_2(\mathrm{SOC_j},i)\cdot C_2(\mathrm{SOC_j},i)}} \cdot R_2\left(\mathrm{SOC_j},i\right)\mathrm{d}i \\
&-\int_0^{i_2} e^{\frac{-t'_{\mathrm{j}}}{R_2(\mathrm{SOC_j},i)\cdot C_2(\mathrm{SOC_j},i)}} \cdot R_2\left(\mathrm{SOC_j},i\right)\mathrm{d}i + \int_0^{i_1} e^{\frac{-t_{\mathrm{j}}}{R_2(\mathrm{SOC_j},i)\cdot C_2(\mathrm{SOC_j},i)}} \cdot R_2\left(\mathrm{SOC_j},i\right)\mathrm{d}i \\
&= \int_{i_1}^{i_2}\left[\begin{array}{r} R_0\left(\mathrm{SOC_j},i\right) + \left(1 - e^{\frac{-(t-t_{\mathrm{j}})}{R_1(\mathrm{SOC_j},i)\cdot C_1(\mathrm{SOC_j},i)}}\right)\cdot R_1\left(\mathrm{SOC_j},i\right) \\ + \left(1 - e^{\frac{-(t-t_{\mathrm{j}})}{R_2(\mathrm{SOC_j},i)\cdot C_2(\mathrm{SOC_j},i)}}\right)\cdot R_2\left(\mathrm{SOC_j},i\right)\end{array}\right]\mathrm{d}i \\
&+\int_0^{i_1} e^{\frac{-t_{\mathrm{j}}}{R_2(\mathrm{SOC_j},i)\cdot C_2(\mathrm{SOC_j},i)}} \cdot \left(1 - e^{\frac{-(t-t_{\mathrm{j}})}{R_2(\mathrm{SOC_j},i)\cdot C_2(\mathrm{SOC_j},i)}}\right)\cdot R_2\left(\mathrm{SOC_j},i\right)\mathrm{d}i \\
&-\int_0^{i_2} e^{\frac{-t'_{\mathrm{j}}}{R_2(\mathrm{SOC_j},i)\cdot C_2(\mathrm{SOC_j},i)}} \cdot \left(1 - e^{\frac{-(t-t_{\mathrm{j}})}{R_2(\mathrm{SOC_j},i)\cdot C_2(\mathrm{SOC_j},i)}}\right)\cdot R_2\left(\mathrm{SOC_j},i\right)\mathrm{d}i
\end{aligned}
\tag{A1}
$$

Appendix B. Derivation of Equation (10)

Under small-signal conditions, *i.e.*, i_1 is very close to i_2 and t_j is very close to t_j', Equation (9) can be transformed as:

$$\begin{aligned}
&U^d(t) - U_{i_2}^c(t) + U_{i_2}^c\left(t_j'\right) - U_{i_1}^c\left(t_j\right)\Big|_{SOC \geqslant SOC_j} \\
&= \int_{i_1}^{i_2} \left[\begin{array}{ll} R_0\left(SOC_j, i\right) & + \left(1 - e^{\frac{-(t-t_j)}{R_1(SOC_j,i)\cdot C_1(SOC_j,i)}}\right)\cdot R_1\left(SOC_j, i\right) \\ & + \left(1 - e^{\frac{-(t-t_j)}{R_2(SOC_j,i)\cdot C_2(SOC_j,i)}}\right)\cdot R_2\left(SOC_j, i\right) \end{array} \right] di \\
&+ \int_0^{i_1} e^{\frac{-t_j}{R_2(SOC_j,i)\cdot C_2(SOC_j,i)}} \cdot \left(1 - e^{\frac{-(t-t_j)}{R_2(SOC_j,i)\cdot C_2(SOC_j,i)}}\right)\cdot R_2\left(SOC_j, i\right) di \\
&- \int_0^{i_2} e^{\frac{-t_j'}{R_2(SOC_j,i)\cdot C_2(SOC_j,i)}} \cdot \left(1 - e^{\frac{-(t-t_j)}{R_2(SOC_j,i)\cdot C_2(SOC_j,i)}}\right)\cdot R_2\left(SOC_j, i\right) di \\
&= \int_{i_1}^{i_2} \left[\begin{array}{ll} R_0\left(SOC_j, i\right) & + \left(1 - e^{\frac{-(t-t_j)}{R_1(SOC_j,i)\cdot C_1(SOC_j,i)}}\right)\cdot R_1\left(SOC_j, i\right) \\ & + \left(1 - e^{\frac{-(t-t_j)}{R_2(SOC_j,i)\cdot C_2(SOC_j,i)}}\right)\cdot R_2\left(SOC_j, i\right) \end{array} \right] di \\
&+ \int_0^{i_1} e^{\frac{-t_j'}{R_2(SOC_j,i)\cdot C_2(SOC_j,i)}} \cdot \left(1 - e^{\frac{-(t-t_j)}{R_2(SOC_j,i)\cdot C_2(SOC_j,i)}}\right)\cdot R_2\left(SOC_j, i\right) di \\
&- \int_0^{i_2} e^{\frac{-t_j'}{R_2(SOC_j,i)\cdot C_2(SOC_j,i)}} \cdot \left(1 - e^{\frac{-(t-t_j)}{R_2(SOC_j,i)\cdot C_2(SOC_j,i)}}\right)\cdot R_2\left(SOC_j, i\right) di
\end{aligned} \tag{B1}$$

with an error of:

$$\begin{aligned}
&\int_0^{i_1} \left(e^{\frac{-t_j}{R_2(SOC_j,i)\cdot C_2(SOC_j,i)}} - e^{\frac{-t_j'}{R_2(SOC_j,i)\cdot C_2(SOC_j,i)}} \right) \cdot \left(1 - e^{\frac{-(t-t_j)}{R_2(SOC_j,i)\cdot C_2(SOC_j,i)}}\right)\cdot R_2\left(SOC_j, i\right) di \\
&\approx \int_0^{i_1} \left(\frac{t_j' - t_j}{R_2\left(SOC_j,i\right)\cdot C_2\left(SOC_j,i\right)} \right) \cdot \left(1 - e^{\frac{-(t-t_j)}{R_2(SOC_j,i)\cdot C_2(SOC_j,i)}}\right)\cdot R_2\left(SOC_j, i\right) di
\end{aligned} \tag{B2}$$

where the second line is derived via Taylor expansion with higher order term neglected. Because t_j is very close to t_j', so the difference divided by R_2C_2 becomes very small and can be neglected. Then, Equation (B3) can be derived from Equation (B1).

$$\begin{aligned}
&U^d(t) - U_{i_2}^c(t) + U_{i_2}^c\left(t_j'\right) - U_{i_1}^c\left(t_j\right)\Big|_{SOC \geqslant SOC_j} \\
&= \int_{i_1}^{i_2} \left[\begin{array}{ll} R_0\left(SOC_j, i\right) & + \left(1 - e^{\frac{-(t-t_j)}{R_1(SOC_j,i)\cdot C_1(SOC_j,i)}}\right)\cdot R_1\left(SOC_j, i\right) \\ & + \left(1 - e^{\frac{-(t-t_j)}{R_2(SOC_j,i)\cdot C_2(SOC_j,i)}}\right)\cdot R_2\left(SOC_j, i\right) \end{array} \right] di \\
&+ \int_0^{i_1} e^{\frac{-t_j'}{R_2(SOC_j,i)\cdot C_2(SOC_j,i)}} \cdot \left(1 - e^{\frac{-(t-t_j)}{R_2(SOC_j,i)\cdot C_2(SOC_j,i)}}\right)\cdot R_2\left(SOC_j, i\right) di \\
&- \int_0^{i_2} e^{\frac{-t_j'}{R_2(SOC_j,i)\cdot C_2(SOC_j,i)}} \cdot \left(1 - e^{\frac{-(t-t_j)}{R_2(SOC_j,i)\cdot C_2(SOC_j,i)}}\right)\cdot R_2\left(SOC_j, i\right) di \\
&\approx \int_{i_1}^{i_2} \left[\begin{array}{c} R_0\left(SOC_j, i\right) + \left(1 - e^{\frac{-(t-t_j)}{R_1(SOC_j,i)\cdot C_1(SOC_j,i)}}\right)\cdot R_1\left(SOC_j, i\right) \\ + \left(1 - e^{\frac{-t_j'}{R_2(SOC_j,i)\cdot C_2(SOC_j,i)}}\right)\cdot \left(1 - e^{\frac{-(t-t_j)}{R_2(SOC_j,i)\cdot C_2(SOC_j,i)}}\right)\cdot R_2\left(SOC_j, i\right) \end{array} \right] di
\end{aligned} \tag{B3}$$

Appendix C. Procedure of Least Square Method

Parameter identification of the ECM under a set of $\{i_1, i_2, SOC_j\}$ is to identify the parameters in Equation (10). Define input and output in Equation (10) as:

$$\begin{aligned}
\widetilde{u}(t) &= i\left(t + t_j\right) - i_1 \\
\widetilde{y}(t) &= U^d\left(t + t_j\right) - U_{i_2}^c\left(t + t_j\right) + U_{i_2}^c\left(t_j\right) - U_{i_1}^c\left(t_j\right)
\end{aligned} \tag{C1}$$

then Equation (10) can be considered as a linear time-invariant system with zero as initial state and initial time. Transfer function of the ECM can be derived from Figure 4 and Equation (10) as:

$$\begin{aligned}
\frac{\widetilde{y}(s)}{\widetilde{u}(s)} &= R_0 + \frac{R_1}{R_1C_1s+1} + \frac{R_2}{R_2C_2s+1} \\
&= \frac{R_0s^2 + \left(\frac{R_0}{R_1C_1} + \frac{R_0}{R_2C_2} + \frac{1}{C_1} + \frac{1}{C_2}\right)s + \frac{R_0+R_1+R_2}{R_1R_2C_1C_2}}{s^2 + \left(\frac{1}{R_1C_1} + \frac{1}{R_2C_2}\right)s + \frac{1}{R_1R_2C_1C_2}} \\
&= \frac{b_2s^2 + b_1s + b_0}{s^2 + a_1s + a_0}
\end{aligned} \tag{C2}$$

where each parametric function is simplified as a letter. Relationships between ECM parameters and transfer function parameters are

$$\left\{ \begin{array}{l}
R_0 = b_2 \\
R_1 = \frac{1}{2}\left(\frac{b_0}{a_0} - b_2\right) + \frac{2a_0b_1 - a_0a_1a_2 - a_1b_0}{2a_0\sqrt{a_1^2 - 4a_0}} \\
C_1 = \frac{a_1 - \sqrt{a_1^2 - 4a_0}}{2a_0}/R_1 \\
R_2 = \frac{1}{2}\left(\frac{b_0}{a_0} - b_2\right) - \frac{2a_0b_1 - a_0a_1a_2 - a_1b_0}{2a_0\sqrt{a_1^2 - 4a_0}} \\
C_1 = \frac{a_1 + \sqrt{a_1^2 - 4a_0}}{2a_0}/R_2
\end{array} \right. \tag{C3}$$

then, Equation (10) can be reformulated as:

$$\widetilde{y}''(t) + a_1\widetilde{y}'(t) + a_0\widetilde{y}(t) = b_2\widetilde{u}''(t) + b_1\widetilde{u}'(t) + b_0\widetilde{u}(t) \tag{C4}$$

where system noise is neglected. At a given time t_k, Equation (C4) can be reformulated to the standard linear regression form as:

$$\widetilde{y}''(t_k) = \varphi^T(t_k)\,\theta \tag{C5}$$

where φ^T and θ are regression vector and parameter vector as:

$$\begin{cases} \varphi^T(t_k) = \begin{bmatrix} -\widetilde{y}'(t_k) & -\widetilde{y}(t_k) & \widetilde{u}''(t_k) & \widetilde{u}'(t_k) & \widetilde{u}(t_k) \end{bmatrix} \\ \theta = \begin{bmatrix} a_1 & a_0 & b_2 & b_1 & b_0 \end{bmatrix}^T \end{cases} \tag{C6}$$

Suppose N samples of input and output data are obtained by experiment and then used for parameter identification with the criterion function of:

$$V_N\left(\theta, Z^N\right) = \frac{1}{N}\sum_{k=1}^{N}\frac{1}{2}\left[\widetilde{y}(t_k) - \varphi^T(t_k)\,\theta\right]^2 \tag{C7}$$

where Z is the dataset with the form of:

$$Z^N = \begin{bmatrix} \varphi^T(t_1) \\ \varphi^T(t_2) \\ \vdots \\ \varphi^T(t_N) \end{bmatrix} \tag{C8}$$

then θ can be estimated with Equation (C9) [50] and ECM parameters can be calculated with Equation (C3).

$$\hat{\theta}_N = \left[\frac{1}{N}\sum_{k=1}^{N}\varphi(t_k)\,\varphi^T(t_k)\right]^{-1}\left[\frac{1}{N}\sum_{k=1}^{N}\varphi(t_k)\,\varphi^T(t_k)\right] \tag{C9}$$

It must be noted that identified R_2 or C_2 needs to be divided or multiplied by the proportional coefficient in the last line of Equation (10) to obtain the true value.

References

1. Lu, L.; Han, X.; Li, J.; Hua, J.; Ouyang, M. A review on the key issues for lithium-ion battery management in electric vehicles. *J. Power Sources* **2013**, *226*, 272–288. [CrossRef]
2. Jossen, A. Fundamentals of battery dynamics. *J. Power Sources* **2006**, *154*, 530–538. [CrossRef]
3. Hu, X.; Li, S.; Peng, H. A comparative study of equivalent circuit models for Li-ion batteries. *J. Power Sources* **2012**, *198*, 359–367. [CrossRef]
4. Abada, S.; Marlair, G.; Lecocq, A.; Petit, M.; Sauvant-Moynot, V.; Huet, F. Safety focused modeling of lithium-ion batteries: A review. *J. Power Sources* **2016**, *306*, 178–192. [CrossRef]
5. Brand, J.; Zhang, Z.; Agarwal, R.K. Extraction of battery parameters of the equivalent circuit model using a multi-objective genetic algorithm. *J. Power Sources* **2014**, *247*, 729–737. [CrossRef]
6. Li, J.; Wang, L.; Lyu, C.; Wang, H.; Liu, X. New method for parameter estimation of an electrochemical-thermal coupling model for $LiCoO_2$ battery. *J. Power Sources* **2015**, *307*, 220–230. [CrossRef]
7. Waag, W.; Fleischer, C.; Sauer, D.U. Critical review of the methods for monitoring of lithium-ion batteries in electric and hybrid vehicles. *J. Power Sources* **2014**, *258*, 321–339. [CrossRef]
8. Feng, F.; Lu, R.; Zhu, C. A combined state of charge estimation method for lithium-ion batteries used in a wide ambient temperature range. *Energies* **2014**, *7*, 3004–3032. [CrossRef]

9. Yuan, S.; Wu, H.; Yin, C. State of charge estimation using the extended Kalman filter for battery management systems based on the ARX battery model. *Energies* **2013**, *4*, 444–470. [CrossRef]
10. Kim, D.; Koo, K.; Jeong, J.J.; Goh, T.; Kim, S.W. Second-order discrete-time sliding mode observer for state of charge determination based on a dynamic resistance Li-ion battery model. *Energies* **2013**, *4*, 5538–5551. [CrossRef]
11. Zhang, X. Thermal analysis of a cylindrical lithium-ion battery. *Electrochim. Acta* **2011**, *56*, 1246–1255. [CrossRef]
12. Guo, M.; Sikha, G.; White, R.E. Single-particle model for a lithium-ion cell: Thermal behavior. *J. Electrochem. Soc.* **2011**, *158*, A122–A132. [CrossRef]
13. Prada, E.; Domenico, D.; Creff, Y.; Bernard, J.; Sauvant-Moynot, V.; Huet, F. Simplified electrochemical and thermal model of $LiFePO_4$-graphite Li-ion batteries for fast charge applications. *J. Electrochem. Soc.* **2012**, *159*, A1508–A1519. [CrossRef]
14. Guo, M.; Kim, G.; White, R.E. A three-dimensional multi-physics model for a Li-ion battery. *J. Power Sources* **2013**, *240*, 80–94. [CrossRef]
15. Nieto, N.; Diaz, L.; Gastelurrutia, J.; Alavam, I.; Blanco, F.; Ramos, J.C.; Rivas, A. Thermal Modeling of Large Format Lithium-Ion Cells. *J. Electrochem. Soc.* **2013**, *160*, A212–A217. [CrossRef]
16. Yi, J.; Koo, B.; Shin, C.B. Three-Dimensional Modeling of the Thermal Behavior of a Lithium-Ion Battery Module for Hybrid Electric Vehicle Applications. *Energies* **2014**, *7*, 7856–7601. [CrossRef]
17. Yazdanpour, M.; Taheri, P.; Mansouri, A.; Bahrami, M. A Distributed Analytical Electro-Thermal Model for Pouch-Type Lithium-Ion Batteries. *J. Electrochem. Soc.* **2014**, *161*, A1953–A1963. [CrossRef]
18. Dees, D.; Gunen, E.; Abraham, D.; Jansen, A.; Prakash, J. Electrochemical Modeling of Lithium-Ion Positive Electrodes during Hybrid Pulse Power Characterization Tests. *J. Electrochem. Soc.* **2008**, *155*, A603–A613. [CrossRef]
19. Albertus, P.; Christensen, J.; Newman, J. Experiments on and Modeling of Positive Electrodes with Multiple Active Materials for Lithium-Ion Batteries. *J. Electrochem. Soc.* **2009**, *156*, A606–A618. [CrossRef]
20. Srinivasan, V.; Newman, J. Design and Optimization of a Natural Graphite/Iron Phosphate Lithium-Ion Cell. *J. Electrochem. Soc.* **2004**, *151*, A1530–A1538. [CrossRef]
21. Doyle, M.; Fuentes, Y. Computer Simulations of a Lithium-Ion Polymer Battery and Implications for Higher Capacity Next-Generation Battery Designs. *J. Electrochem. Soc.* **2003**, *150*, A706–A713. [CrossRef]
22. Zhu, J.G.; Sun, Z.C.; Wei, X.Z.; Dai, H.F. A new lithium-ion battery internal temperature on-line estimate method based on electrochemical impedance spectroscopy measurement. *J. Power Sources* **2015**, *274*, 990–1004. [CrossRef]
23. Gomez, J.; Nelson, R.; Kalu, E.; Weatherspoon, M.H.; Zheng, J.P. Equivalent circuit model parameters of a high-power Li-ion battery: Thermal and state of charge effects. *J. Power Sources* **2011**, *196*, 4826–4831. [CrossRef]
24. Lin, X.; Perez, H.E.; Mohan, S.; Siegel, J.B.; Stefanopoulou, A.G.; Ding, Y.; Castanier, M.P. A lumped-parameter electro-thermal model for cylindrical batteries. *J. Power Sources* **2014**, *257*, 1–11. [CrossRef]
25. Murashko, K.; Pyrhönen, J.; Laurila, L. Three-dimensional thermal model of a lithium ion battery for hybrid mobile working machines: Determination of the model parameters in a pouch cell. *IEEE Trans. Energy Convers.* **2013**, *28*, 335–343. [CrossRef]
26. Alaoui, C. Solid-state thermal management for lithium-ion EV batteries. *IEEE Trans. Veh. Technol.* **2013**, *62*, 98–107. [CrossRef]
27. Vertiz, G.; Oyarbide, M.; Macicior, H.; Miguel, O.; Cantero, I.; Arroiabe, P.F.; Ulacia, I. Thermal characterization of large size lithium-ion pouch cell based on 1d electro-thermal model. *J. Power Sources* **2014**, *272*, 476–484. [CrossRef]
28. *Lithium Ion Cells and Batteries Used in Portable Electronic Equipments: Safety Requirements*; GB 31241-2014; Standards Press of China: Beijing, China, 2014.
29. Wu, B.; Yufit, V.; Marinescu, M.; Offer, G.J.; Martinez-Botas, R.F.; Brandon, N.P. Coupled thermal electrochemical modelling of uneven heat generation in lithium-ion battery packs. *J. Power Sources* **2013**, *243*, 544–554. [CrossRef]
30. Buller, S.; Thele, M.; Karden, E. Impedance-based non-linear dynamic battery modeling for automotive applications. *J. Power Sources* **2003**, *113*, 422–430. [CrossRef]

31. Andre, D.; Meiler, M.; Steiner, K.; Wimmer, Ch.; Soczka-Guth, T.; Sauer, D.U. Characterization of high-power lithium-ion batteries by electrochemical impedance spectroscopy I: Experimental investigation. *J. Power Sources* **2011**, *196*, 5334–5341. [CrossRef]
32. Andre, D.; Meiler, M.; Steiner, K.; Wimmer, Ch.; Soczka-Guth, T.; Sauer, D.U. Characterization of high-power lithium-ion batteries by electrochemical impedance spectroscopy II: Modelling. *J. Power Sources* **2011**, *196*, 5349–5356. [CrossRef]
33. Schmidt, J.P.; Chrobak, T.; Ender, M.; Illig, J.; Klotz, D.; Ivers-Tiffée, E. Studies on $LiFePO_4$ as cathode material using impedance spectroscopy. *J. Power Sources* **2011**, *196*, 5342–5348. [CrossRef]
34. Fleischer, C.; Waag, W.; Heyn, H.M.; Sauer, D.U. On-line adaptive battery impedance parameter and state estimation considering physical principles in reduced order equivalent circuit battery models: Part 1. Requirements critical review of methods and modeling. *J. Power Sources* **2014**, *260*, 276–291. [CrossRef]
35. Fleischer, C.; Waag, W.; Heyn, H.M.; Sauer, D.U. On-line adaptive battery impedance parameter and state estimation considering physical principles in reduced order equivalent circuit battery models: Part 2. Parameter and state estimation. *J. Power Sources* **2014**, *262*, 457–482. [CrossRef]
36. Roscher, M.A.; Sauer, D.U. Dynamic electric behavior and open-circuit-voltage modeling of $LiFePO_4$-based lithium ion secondary batteries. *J. Power Sources* **2011**, *196*, 331–336. [CrossRef]
37. Chiang, Y.H.; Sean, W.Y.; Ke, J.C. Online estimation of internal resistance and open-circuit voltage of lithium-ion batteries in electric vehicles. *J. Power Sources* **2011**, *196*, 3921–3932. [CrossRef]
38. Roscher, M.A.; Assfalg, J.; Bohlen, O.S. Detection of utilizable capacity deterioration in battery systems. *IEEE Trans. Veh. Technol.* **2011**, *60*, 98–103. [CrossRef]
39. He, H.; Xiong, R.; Zhang, X.; Sun, F.; Fan, J. State-of-charge estimation of the lithium-ion battery using an adaptive extended Kalman filter based on an improved Thevenin model. *IEEE Trans. Veh. Technol.* **2011**, *60*, 1461–1469.
40. Pattipati, B.; Sankavaram, C.; Pattipati, K.R. System identification and estimation framework for pivotal automotive battery management system characteristics. *IEEE Trans. Syst. Man Cybern. Part C Appl. Rev.* **2011**, *41*, 869–884. [CrossRef]
41. Electric Vehicle Battery Test Procedures Manual. Available online: http://avt.inl.gov/battery/pdf/usabc_manual_rev2.pdf (accessed on 2 December 2015).
42. Battery Test Manual or Plug-In Hybrid Electric Vehicles. Available online: https://inldigitallibrary.inl.gov/sti/3952791.pdf (accessed on 1 June 2016).
43. Negative Resistance. Available online: https://en.wikipedia.org/wiki/Negative_resistance (accessed on 13 March 2016).
44. Grassi, R.; Gnudi, A.; Lecce, V.D.; Gnani, E.; Reggiani, S.; Baccarani, G. Exploiting negative differential resistance in monolayer graphene FETs for high voltage gains. *IEEE Trans. Electron. Devices* **2014**, *61*, 617–624. [CrossRef]
45. Ershov, M.; Liu, H.C.; Buchanan, M.; Wasilewski, Z.R.; Jonscher, A.K. Negative capacitance effect in semiconductor devices. *IEEE Trans. Electron. Devices* **1998**, *45*, 2196–2206. [CrossRef]
46. Negative Impedance Converter. Available online: https://en.wikipedia.org/wiki/Negative_impedance_converter (accessed on 21 April 2016).
47. Jain, A.; Alam, M.A. Stability constraints define the minimum subthreshold swing of a negative capacitance field-effect transistor. *IEEE Trans. Electron. Devices* **2014**, *61*, 2235–2242. [CrossRef]
48. Bard, A.J.; Faulkner, L.R. *Electrochemical Methods: Fundamentals and Applications*, 2nd ed.; John Wiley & Sons Inc.: New York, NY, USA, 2001; pp. 161–168.
49. Hu, Y.; Yurkovich, S. Linear parameter varying battery model identification using subspace methods. *J. Power Sources* **2011**, *196*, 2913–2923. [CrossRef]
50. Garnier, H.; Mensler, M.; Richard, A. Continuous-time model identification from sampled data: Implementation issues and performance evaluation. *Int. J. Control* **2003**, *76*, 1337–1357. [CrossRef]